Understanding Kickmaps

October 24, 2014

Ward A. Wurtz

Canadian Light Source Inc.
101 Perimeter Road
University of Saskatchewan
Saskatoon, Saskatchewan
S7N 0X4 Canada

Contents

Typeset in LaTeX

1 Introduction

The purpose of this document is to help the reader better understand kickmaps. A kickmap is a numerical technique used to model insertion devices for use in charged particle transport codes. It was first developed by P. Elleaume at ESRF [1, 2] and has been adopted by many laboratories. The input to the kickmap technique is a 3D magnetic model of an insertion device. The output are functions $\Delta x'(x,z)$ and $\Delta z'(x,z)$ which give the resulting horizontal and vertical kicks to an electron at horizontal position x and vertical position z. The functions $\Delta x'(x,z)$ and $\Delta z'(x,z)$ are the kickmaps.

The kickmap method is derived from the Lorentz force law. We discuss the derivation of a specialized equation of motion from the Lorentz force law in Section 2 and then obtain the kickmap equations in Section 3.

We discuss the calculation of kickmaps using the numerical methods of the magnetostatics code RADIA [3] and their incorporation into the charged particle transport code elegant [4] in Section 4. While we always compute kickmaps numerically in practice, there is a great deal that can be learned by an analytical treatment. We examine common features of kickmaps for planar insertion devices in Section 5 and for elliptically polarizing undulators (EPUs) in Section 6. In these sections, we compare our analytic results with numerical calculations for actual insertion devices under development for CLS.

The goal of this document is to provide a reader with an improved understanding of the kickmap technique. We try to build an intuitive understanding of the techniques as we move through technical details. During the kickmap derivation, we may sacrifice some rigour in order to improve understanding. Rest assured that the ESRF report by P. Elleaume contains a thoroughly rigourous treatment of the derivation [2]. When we discuss planar devices and EPUs, we will try to use a combination of numeric results (i.e. pictures) and analytic expressions to build understanding and intuition. I hope that reading this report helps you to better understand kickmaps, as writing it did for me.

2 Equations of Motion

In order to derive the kickmap equations, we must first derive the equations of motion in a useful form. We will then look at some simple approximations to the equations of motion.

2.1 Derivation of the Equations of Motion

We begin by defining a coordinate system, shown in Figure 2.1 . We chose our coordinate system to be consis-

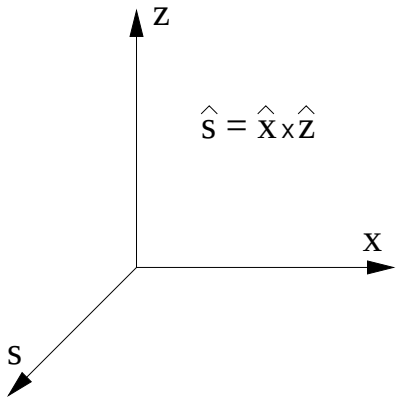

Figure 2.1: Laboratory frame coordinate system

tent with the kickmap papers of Elleaume [1]. In this coordinate system, x is the horizontal coordinate, z is the

vertical coordinate and s is the longitudinal coordinate. The horizontal coordinate is defined such that $x > 0$ is the outboard direction and $x < 0$ is the inboard direction. The vertical coordinate is defined such that $z > 0$ is up. The longitudinal coordinate is defined such that the electron travels in the positive direction. This coordinate system works for a machine where the electrons go counter-clockwise when viewed from above giving a cross product of $\hat{s} = \hat{x} \times \hat{z}$.

We begin our derivation from the relativistic Lorentz-force law,

$$\frac{d\vec{p}}{dt} = q\vec{v} \times \vec{B} \tag{2.1}$$

where $\vec{p}$ is the momentum of the electron, $q = -e$ is the electron's charge, $\vec{v}$ is the electron's velocity and $\vec{B}$ is the magnetic field along the electron's path. We can write the electron's velocity as

$$\begin{aligned} \vec{v} &= \frac{dx}{dt}\hat{x} + \frac{dz}{dt}\hat{z} + \frac{ds}{dt}\hat{s} \\ &= \left(\frac{ds}{dt}\right)\left(\frac{dx}{ds}\hat{x} + \frac{dz}{ds}\hat{z} + \hat{s}\right). \end{aligned} \tag{2.2}$$

If we define

$$x' \equiv \frac{dx}{ds} \text{ and } z' \equiv \frac{dz}{ds} \tag{2.3}$$

and assume that the electron is ultra-relativistic and are essentially going the speed of light, c (i.e. $\beta = 1$) then

$$c^2 = \vec{v}^2 = \left(\frac{ds}{dt}\right)^2 \left(x'^2 + z'^2 + 1\right). \tag{2.4}$$

Solving for ds/dt gives an expression of

$$\vec{v} = \frac{c}{\sqrt{x'^2 + z'^2 + 1}} \left(x'\hat{x} + z'\hat{z} + \hat{s}\right) \tag{2.5}$$

for the electron's velocity. We substitute this into the Lorentz force law, equation 2.1, to obtain

$$\frac{d\vec{p}}{dt} = \frac{-ec}{\sqrt{x'^2 + z'^2 + 1}} \left[\left(z'B_s - B_z\right)\hat{x} - \left(x'B_s - B_x\right)\hat{z} + \left(x'B_z - z'B_x\right)\hat{s}\right] \tag{2.6}$$

where $\vec{B} = B_x\hat{x} + B_z\hat{z} + B_s\hat{s}$. This equation represents the Lorentz force law in the coordinate system defined in Figure 2.1. Because we have fixed the electrons speed as the speed of light, we have only two velocity degrees of freedom remaining, x' and z'. It is trivial to note that $s' = ds/ds = 1$. Also note that the time variable has been completely removed from the right-hand side of equation 2.6.

We have assumed that the velocity of the electron is indistinguishable from the speed of light. However, the energy of the electrons is not infinite, and we calculate

$$\gamma \equiv \frac{E_e}{m_e c^2} \tag{2.7}$$

where E_e is the electron's total energy[1] and m_e is the electron's rest mass. The momentum of a relativistic electron is

$$\vec{p} = \gamma m_e \vec{v} = \frac{\gamma m_e c}{\sqrt{x'^2 + z'^2 + 1}} \left(x'\hat{x} + z'\hat{z} + \hat{s}\right) \tag{2.8}$$

and it's time derivative is

$$\begin{aligned} \frac{d\vec{p}}{dt} &= \frac{ds}{dt}\frac{d\vec{p}}{ds} \\ &= \frac{\gamma m_e c^2}{\sqrt{x'^2 + z'^2 + 1}} \left[-\frac{1}{2}\left(x'^2 + z'^2 + 1\right)^{-\frac{3}{2}} \left(2x'x'' + 2z'z''\right)\left(x'\hat{x} + z'\hat{z} + \hat{s}\right) \right. \\ &\quad \left. + \frac{x''\hat{x} + z''\hat{z}}{\sqrt{x'^2 + z'^2 + 1}} \right]. \end{aligned} \tag{2.9}$$

[1] The electron is ultra-relativistic so its total energy will be essentially its kinetic energy.

To determine a final form of our equations of motion, we must compare the vector components of equation 2.6 with those of equation 2.9. Both equations provide an expression for the time rate of change of the electron's momentum. Equation 2.6 was derived using the Lorentz force law while equation 2.9 was derived using only kinematics.

We can equate the longitudinal coordinates (i.e. $\hat{s}$) of equations 2.6 and 2.9 to find

$$\frac{x'x'' + z'z''}{(x'^2 + z'^2 + 1)^{\frac{3}{2}}} = \alpha \left(x'B_z - z'B_x\right) \tag{2.10}$$

where $\alpha \equiv e/\gamma mc$. After substituting equation 2.10 into equation 2.9 the remaining two vector components are related by

$$-\alpha \left(x'B_z - z'B_x\right)\left(x'\hat{x} + z'\hat{z}\right) + \frac{x''\hat{x} + z''\hat{z}}{\sqrt{x'^2 + z'^2 + 1}} = -\alpha\left[\left(z'B_s - B_z\right)\hat{x} - \left(x'B_s - B_x\right)\hat{z}\right]. \tag{2.11}$$

We can solve this equation for x'' and z'' and find

$$x'' = -\alpha\sqrt{x'^2 + z'^2 + 1}\left(z'B_s + x'z'B_x - (1 + x'^2)B_z\right) \tag{2.12}$$

$$z'' = -\alpha\sqrt{x'^2 + z'^2 + 1}\left(-x'B_s - x'z'B_z + (1 + z'^2)B_x\right) \tag{2.13}$$

which are the required equations of motion[2].

Given a relativistic electron at initial position s_0 with initial phase space coordinates x_0, z_0, x'_0 and z'_0 and a magnetic field vector $\vec{B}(x, z, s)$ we can use these equations of motion to calculate the phase-space trajectory of the electron, $x(s)$, $z(s)$, $x'(s)$ and $z'(s)$, as it passes through the magnetic field.

2.2 First-Order Solutions to the Equations of Motion

The equations of motion in equations 2.12 and 2.13 can be used for numerical tracking of a particle traveling through a magnetic field region. However, a more thorough analysis is needed to optimize them for use in a particle tracking code.

We begin by examining a trivial case where we neglect all transverse acceleration of the electrons. The equations of motion reduce to $z'' = 0$ and $x'' = 0$. The trajectory of the electrons is then $x(s) = x'_0 s + x_0$ and $z(s) = z'_0 s + z_0$. This is the trajectory of an electron traveling through a drift space.

A more interesting solution can be found by neglecting all x' and z' terms of the equations of motion, assuming that the transverse motion of the electrons is small. The equations of motion then reduce to

$$x'' = \alpha B_z \text{ and } z'' = -\alpha B_x. \tag{2.14}$$

We see immediately that these equations obey the right-hand rule[3] as defined by our coordinate system in Figure

[2] Note that the equations of motion reported in [1] have an error. The factor $\sqrt{x'^2 + z'^2 + 1}$ is shown to be in the denominator whereas it should be in the numerator. Reference [2] agrees with equations 2.12 and 2.13.

[3] Remember, electrons have negative charge.

2.1. The solutions to these linear equations of motion are

$$\begin{aligned} x'(s) &= \alpha \int_{-\infty}^{s} B_z(0,0,s')ds' \\ z'(s) &= -\alpha \int_{-\infty}^{s} B_x(0,0,s')ds' \\ x(s) &= \alpha \int_{-\infty}^{s}\int_{-\infty}^{s'} B_z(0,0,s'')ds''ds' \\ z(s) &= -\alpha \int_{-\infty}^{s}\int_{-\infty}^{s'} B_x(0,0,s'')ds''ds' \end{aligned} \tag{2.15}$$

where we have chosen our coordinate system such that all initial phase-space coordinates are zero and the symbol $-\infty$ in a convention to mean at the beginning of the area of interest.

In the first-order, the equations of motion depend only on the magnetic field and not on the transverse motion of the electrons through this field. This is a good approximation for lattice elements like quadrupole and sextupole magnets. The effects of the field integrals on the electron add as it passes through the device.

However, insertion devices are a different story. While field integrals inside an insertion device are non-zero, insertion devices are designed with field integrals at the end of the device as close to zero as possible. The first-order solutions to the equations of motion suggest that the insertion device would then function as a drift space. However, we know from tune shift measurements that even an ideal, planar insertion device has a vertical focusing effect on the electron beam. This effect is due to the second-order terms of the equations of motion, which are the basis of the kickmap technique.

3 Derivation of Kickmap Formula

3.1 Second-Order Solutions to the Equations of Motion

In Section 2.1 we derived the equations of motion, given in equations 2.12 and 2.13, and reproduced here

$$\begin{aligned} x'' &= -\alpha\sqrt{x'^2+z'^2+1}\left(z'B_s + x'z'B_x - (1+x'^2)B_z\right) \\ z'' &= -\alpha\sqrt{x'^2+z'^2+1}\left(-x'B_s - x'z'B_z + (1+z'^2)B_x\right) \end{aligned}$$

where $\alpha \equiv e/\gamma m_e c^2 = e/|\vec{p}| = 1/B\rho$ where $B\rho$ is the magnetic rigidity. In Section 2.2 we looked at the first-order solutions to the equations of motion where we neglected all transverse motion of the electron beam. While these equations may be suitable for a quadrupole magnet, they are not suitable for an insertion device because the first and second field integrals over the entire device are very small by design. In other words, we take

$$\int_{-\infty}^{\infty} B_z ds = 0 \text{ and } \int_{-\infty}^{\infty} B_x ds = 0 \tag{3.1}$$

for insertion devices when integrating over the entire device[4]. It is important to note that, inside the device, the field integrals are not zero and the first-order solutions are dominant. It is only when we integrate over the entire device that the first-order solutions are zero.

[4] Recall that we use the symbol $-\infty$ to mean before the device and ∞ to mean after the device.

We will derive the kickmap equations by retaining terms with a single phase-space coordinate and neglect those with multipole phase-space coordinates. For instance, we will keep all terms with x' but will neglect terms like x'^2, x^2 and $x'z'$. In the literature, the kickmap derivation is often said to keep terms of "second order of the inverse of the electron energy" [1]. Looking at equations 2.15, we can see that the phase space variables are all proportional to α, which is essentially the inverse of electron energy as $\alpha = ec/E_e$. Thus, terms like $\alpha x'$ are second-order of the inverse energy, and these are the terms that we will keep in our equations of motion. We chose our derivation because it is conceptually easier and our goal is to understand the mathematics of kickmaps at the expense of some mathematical rigour.

If we neglect all terms with multiple phase-space variables, our equations of motion become

$$\begin{aligned} x'' &= -\alpha\left(z' B_s - B_z\right) \\ z'' &= -\alpha\left(B_x - x' B_s\right). \end{aligned} \tag{3.2}$$

We note that we have the magnetic field B_x and B_z appearing explicitly in equation 3.2. Since we are not neglecting the transverse motion of the electrons, we must consider that these fields may vary as the electrons move transversely through them. To this end, we will use the Taylor expansion of the fields

$$\begin{aligned} B_z(x,z,s) &= B_z(0,0,s) + x\frac{\partial B_z}{\partial x}(0,0,s) + z\frac{\partial B_z}{\partial z}(0,0,s) + \ldots \\ B_x(x,z,s) &= B_x(0,0,s) + x\frac{\partial B_x}{\partial x}(0,0,s) + z\frac{\partial B_x}{\partial z}(0,0,s) + \ldots \end{aligned} \tag{3.3}$$

and find that the coordinates x and z appear. Since we are keeping terms with single phase-space variables and neglecting those with multiple phase-space variables, we are able to truncate the Taylor expansions as shown. In other words, we neglect the higher order terms containing x^2, z^2 and xz. Combining equations 3.2 and 3.3 we have second-order equations of motion

$$\begin{aligned} x'' &= -\alpha\left(z' B_s^0 - B_z^0 - x\frac{\partial B_z^0}{\partial x} - z\frac{\partial B_z^0}{\partial z}\right) \\ z'' &= -\alpha\left(B_x^0 + x\frac{\partial B_x^0}{\partial x} + z\frac{\partial B_x^0}{\partial z} - x' B_s^0\right). \end{aligned} \tag{3.4}$$

where we have defined $B_x^0(s) \equiv B_x(0,0,s)$, $\partial B_z^0/\partial x(s) \equiv \partial B_z/\partial x(0,0,s)$, etc. It is important to recall at this point that we have chosen our coordinate system such that the initial phase space variables are all zero: $x_0 = 0$, $z_0 = 0$, $x_0' = 0$ and $z_0' = 0$. One may also wonder why we did not perform a Taylor expansion for B_s as we did for B_x and B_z. This is because B_s is multiplied by a phase space variable in the equation of motion; only the first-order term of the Taylor expansion, B_s^0, is retained.

We now eliminate all phase space variables from equation 3.4. The purpose of an insertion device is to cause the electrons to wiggle or undulate, hence the names wiggler and undulator. Inside of the insertion device, the electrons undergo transverse motion which is dominated by the first-order equations of motion of equation 2.15. It is only when we integrate over the entire device that the first-order equations of motion give us a negligible effect on the electrons, as represented by equation 3.1. If we insert the first-order equations of motion, equations 2.15, into our second-order equations of motion, equation 3.4, integrate over the device and require the field integrals to be zero, we obtain

$$\begin{aligned} \Delta x' &\equiv \int_{-\infty}^{\infty} x''ds = \alpha^2 \int_{-\infty}^{\infty}\left[B_s^0\int_{-\infty}^{s} B_x^0 ds' + \frac{\partial B_z^0}{\partial x}\int_{-\infty}^{s}\int_{-\infty}^{s'} B_z^0 ds'' ds' - \frac{\partial B_z^0}{\partial z}\int_{-\infty}^{s}\int_{-\infty}^{s'} B_x^0 ds'' ds'\right] ds \\ \Delta z' &\equiv \int_{-\infty}^{\infty} z''ds = \alpha^2 \int_{-\infty}^{\infty}\left[B_s^0\int_{-\infty}^{s} B_z^0 ds' + \frac{\partial B_x^0}{\partial z}\int_{-\infty}^{s}\int_{-\infty}^{s'} B_x^0 ds'' ds' - \frac{\partial B_x^0}{\partial x}\int_{-\infty}^{s}\int_{-\infty}^{s'} B_z^0 ds'' ds'\right] ds \end{aligned} \tag{3.5}$$

as our solution to the second-order equations of motion. Equation 3.5 is the kickmap equation. In order to obtain the form typically seen in the literature, we must apply Maxwell's equations and integration by parts, and we will

do this in the next section. We should take a moment to better understand the origin of kickmaps by examining equations 3.4 and 3.5.

When we speak of the effect of an insertion device on the electron beam, we use the word ‘dynamic’ to describe the effect. We often speak of ‘dynamic focusing’. The term ‘dynamic multipoles’ is used by some, but it must be understood that the focusing effects of a kickmap do not obey the multipole expansion. The term ‘dynamic’ is used because, without the transverse motion of the electron through the insertion device, equation 3.5 is zero. When there is transverse motion through a complex magnetic field, the kickmap equations introduce dynamic effects that may have a complex, nonlinear structure.

There are three terms within the main integral of equation 3.5. The first term represents the transverse motion of the electrons through a longitudinal magnetic field. The second and third terms represent the varying transverse position of the electron as it moves through a varying magnetic field. These two, competing sources of dynamic effects can create very complex dynamics for an electron beam.

While great physical insight can be found in equation 3.5, it is not computationally effective. We will apply Maxwell’s equations and integration by parts to obtain a form that is more useful in calculations.

3.2 Applying Maxwell’s Equations and Integration by Parts

In order to make kickmaps easier to calculate, we will apply Maxwell’s equations and integration of parts to equation 3.5. In this report, we will look only at the $\Delta x'$ equation as the $\Delta z'$ equation proceeds exactly the same.

To simplify the first term of equation 3.5, we will use the fact that the divergence of the magnetic field in free space is zero. In other words

$$\frac{\partial B_x^0}{\partial x} + \frac{\partial B_z^0}{\partial z} + \frac{\partial B_s^0}{\partial s} = 0 \tag{3.6}$$

allowing us to write

$$B_s^0 = \int_{-\infty}^{s} \frac{\partial B_s^0}{\partial s'} ds' = -\int_{-\infty}^{s} \frac{\partial B_x^0}{\partial x} ds' - \int_{-\infty}^{s} \frac{\partial B_z^0}{\partial z} ds' \tag{3.7}$$

which we can use to eliminate B_s^0 from equation 3.5.

The second term of equation 3.5 can be simplified by using integration by parts,

$$\int_a^b f(s)g'(s)ds = [f(s)g(s)]_a^b - \int_a^b f'(s)g(s)ds. \tag{3.8}$$

Including the overall integral, the second term can be written as

$$\begin{aligned} \int_{-\infty}^{\infty} \left[\frac{\partial B_z^0}{\partial x} \int_{-\infty}^{s} \int_{-\infty}^{s'} B_z^0 ds'' ds' \right] ds &= \left[\int_{-\infty}^{s} \frac{\partial B_z^0}{\partial x} ds' \int_{-\infty}^{s} \int_{-\infty}^{s'} B_z^0 ds'' ds' \right]_{-\infty}^{\infty} - \int_{-\infty}^{\infty} \left[\int_{-\infty}^{s} \frac{\partial B_z^0}{\partial x} ds' \int_{-\infty}^{s} B_z^0 ds' \right] ds \\ &= -\int_{-\infty}^{\infty} \left[\int_{-\infty}^{s} \frac{\partial B_z^0}{\partial x} ds' \int_{-\infty}^{s} B_z^0 ds' \right] ds \end{aligned} \tag{3.9}$$

using the fact that the second field integral over the device is zero by design. Using integration by parts, the third term can be simplified to

$$\int_{-\infty}^{\infty} \left[\frac{\partial B_z^0}{\partial z} \int_{-\infty}^{s} \int_{-\infty}^{s'} B_x^0 ds'' ds' \right] ds = -\int_{-\infty}^{\infty} \left[\int_{-\infty}^{s} \frac{\partial B_z^0}{\partial z} ds' \int_{-\infty}^{s} B_x^0 ds' \right] ds. \tag{3.10}$$

We can now combine the three simplified terms into the equation 3.5 to obtain

$$\begin{aligned}\Delta x' &= \alpha^2 \int_{-\infty}^{\infty} \left[-\int_{-\infty}^{s} \frac{\partial B_x^0}{\partial x} ds' \int_{-\infty}^{s} B_x^0 ds' - \int_{-\infty}^{s} \frac{\partial B_z^0}{\partial z} ds' \int_{-\infty}^{s} B_x^0 ds' \right. \\ &\quad \left. - \int_{-\infty}^{s} \frac{\partial B_z^0}{\partial x} ds' \int_{-\infty}^{s} B_z^0 ds' + \int_{-\infty}^{s} \frac{\partial B_z^0}{\partial z} ds' \int_{-\infty}^{s} B_x^0 ds' \right] ds \\ &= -\frac{\alpha^2}{2} \int_{-\infty}^{\infty} \frac{\partial}{\partial x} \left[\left(\int_{-\infty}^{s} B_x^0 ds' \right)^2 + \left(\int_{-\infty}^{s} B_z^0 ds' \right)^2 \right] ds. \end{aligned} \tag{3.11}$$

Likewise, we can obtain a similar equation for the vertical kick

$$\Delta z' = -\frac{\alpha^2}{2} \int_{-\infty}^{\infty} \frac{\partial}{\partial z} \left[\left(\int_{-\infty}^{s} B_x^0 ds' \right)^2 + \left(\int_{-\infty}^{s} B_z^0 ds' \right)^2 \right] ds \tag{3.12}$$

as the equations for the horizontal and vertical kicks are the same with the x and z symbols swapped. It is interesting to note that the only difference between the equations for $\Delta x'$ and $\Delta z'$ is that the derivative is taken in the horizontal and vertical directions, respectively.

We also take a moment to consider our coordinate system. We have defined our coordinate system such that the initial phase space coordinates are always zero. When we apply the kickmap technique to a real beam dynamics problem, this will obviously not be the case. Instead, we will define the coordinate system such that $x = 0$ and $z = 0$ are on the closed orbit at either end of the insertion device. Therefore, we must apply the kickmap equations at each x and z giving us functions $\Delta x'(x, z)$ and $\Delta z'(x, z)$; this puts the 'map' into 'kickmap'. As a result, we will write the magnetic field components without the '0' superscript. Our final form of the kickmaps equations is given here,

$$\Phi(x, z, s) \equiv \left(\int_{-\infty}^{s} B_x(x, z, s') ds' \right)^2 + \left(\int_{-\infty}^{s} B_z(x, z, s') ds' \right)^2 \tag{3.13}$$

$$\Delta x'(x, z) = -\frac{\alpha^2}{2} \int_{-\infty}^{\infty} \frac{\partial \Phi}{\partial x}(x, z, s) ds \tag{3.14}$$

$$\Delta z'(x, z) = -\frac{\alpha^2}{2} \int_{-\infty}^{\infty} \frac{\partial \Phi}{\partial z}(x, z, s) ds. \tag{3.15}$$

Equations 3.13, 3.14 and 3.15 will collectively be referred to as the kickmap equations, and we recall here that $\alpha \equiv e/\gamma m_e c^2 = e/|\vec{p}| = 1/B\rho$ where $B\rho$ is the magnetic rigidity. This form simplifies both analytic and numerical computations.

When a kickmap is implemented, we must consider the finite length of the device. Some of the electrons incident on the insertion device will have non-zero transverse velocity $x' \neq 0$ and $z' \neq 0$. Up until now, we have assumed that the electrons have no initial transverse velocity. Also, the machine beta functions vary across the device and this variation must be considered when calculating quantities such as tune shifts. Therefore, when we implement kickmaps in actual calculations, we break the insertion device into pieces. The kickmap can then be implemented as a series of thin lenses along the length of the device. Each thin lens will provide an equal fraction of the kicks $\Delta x'(x, z)$ and $\Delta z'(x, z)$.

We have derived the kickmap equations from the equations of motion which were themselves derived from the Lorentz force law. We have assumed that the electrons are ultra-relativistic, the transverse motion of the

electrons in the insertion device is small but non-negligible and that the insertion device is designed so that the first and second field integrals over the entire device are zero. In return, the kickmap equations give us a means to calculate the dynamic focusing of an insertion device on the stored electrons. Unlike a multipole magnet, where the kick strength is linearly proportional to the magnetic field and α, the strength of a kickmap is proportional to the square of the magnetic field and α. For instance, increasing the magnetic field strength will cause the electrons to have a higher oscillation amplitude through a stronger magnetic field, which gives us the squaring effect.

The remainder of this report will examine the application of the kickmap equations to analytic and numerical calculations involving insertion devices. This will provide us with insight into the effect of insertion devices on electron beam dynamics.

4 Numerical Calculations

Now that we have derived the kickmap equations, equations 3.13, 3.14 and 3.15, we can discuss how to calculate kickmaps and use them in numerical computations to predict the effects of an insertion device on electron beam dynamics.

In Section 4.1 we will discuss a technical problem: when computing a kickmap, does it matter which way we integrate through the insertion device. While this question may seem somewhat esoteric, it has computational importance when computing kickmaps using RADIA and will simplify later analytic calculations. RADIA is a 3D magnetostatics code written at the European Synchrotron Radiation Facility (ESRF) and its use is ubiquitous in insertion device design. We discuss the calculations of kickmaps using RADIA in Section 4.2. Once we create a kickmap using RADIA, we can then import it into a charged particle transport program, such as elegant [4], which we discuss in Section 4.3.

4.1 Integration Direction

In our derivation of the kickmap equations, we reduced a dynamics problem to longitudinal integrals over the transverse magnetic fields and their derivatives. The question we wish to ask here is whether or not it matters which direction we integrate through the device. This result will have important consequences when we compute kickmaps in Section 4.2.

We begin by mirroring the magnetic field in the longitudinal plane,

$$\vec{B}(x,z,s) \rightarrow \vec{B}(x,z,-s) \tag{4.1}$$

which is equivalent to changing the direction of integration. We will use the result

$$\int_a^b f(x)dx = \int_{-b}^{-a} f(-x)dx \tag{4.2}$$

to calculate the transformation of the kickmap potential,

$$\begin{aligned}
\Phi(x,z,s) &\rightarrow \left(\int_{-\infty}^{s} B_x(x,z,-s')ds'\right)^2 + \left(\int_{-\infty}^{s} B_z(x,z,-s')ds'\right)^2 \\
&= \left(\int_{-s}^{\infty} B_x(x,z,s')ds'\right)^2 + \left(\int_{-s}^{\infty} B_z(x,z,s')ds'\right)^2 \text{ (by equation 4.2)} \\
&= \left(\int_{-\infty}^{-s} B_x(x,z,s')ds'\right)^2 + \left(\int_{-\infty}^{-s} B_z(x,z,s')ds'\right)^2 \text{ (by equation 3.1)} \\
&= \Phi(x,z,-s) \qquad (4.3)
\end{aligned}$$

which leads to the transformation of the kickmap

$$\begin{aligned}
\Delta x'(x,z) &\rightarrow -\frac{\alpha^2}{2}\int_{-\infty}^{\infty} \frac{\partial\Phi}{\partial x}(x,z,-s)ds \\
&= -\frac{\alpha^2}{2}\int_{-\infty}^{\infty} \frac{\partial\Phi}{\partial x}(x,z,s)ds \text{ (by equation 4.2)} \\
&= \Delta x'(x,z). \qquad (4.4)
\end{aligned}$$

Likewise $\Delta z'(x,z) \rightarrow \Delta z'(x,z)$. Therefore, as long as the field integrals are zero, the kickmap does not care which way we integrate through the insertion device.

4.2 Calculating Kickmaps with RAIDA

RADIA [3] is a 3D magnetostatics code which runs in Wolfram Mathematica. It is used in the design of insertion devices. RADIA uses numerical methods to calculate the magnetic field due to an insertion device. It can then use the calculated magnetic field to calculate kickmaps.

There are two functions to calculate kickmaps in RADIA: a function which integrates over one period of the device and another which integrates over the entire device. Generally, since insertion devices are periodic, and the end pole design typically has a small effect on the kickmap, it is sufficient to calculate the kickmap using a single period and then have RADIA multiply it by the number of periods. The ability to calculate kickmaps by integrating over the entire device is useful if you wish to verify that the ends of the device do not have a great effect or to verify that the periodic calculation is configured correctly. In these cases, it is sufficient to perform the non-periodic calculation at only a few points. The Mathematica help for each function can be found using the '?' command:

?radFldFocKick

radFldFocKick[obj,{x1,y1,z1},{nsx,nsy,nsz},{ds1,ds2,ds3,...},nps,{n1x,n1y,n1z},r1,np1,r2,np2,com:"",{d1:0,d2:0}]

> Computes matrices of 2nd order kicks of trajectory of relativistic charged particle in arbitrary magnetic field produced by the object obj. PLEASE NOTE that this is a time-consuming calculation; therefore try using the radFldFocKickPer function were applicable. The longitudinal integration starts at point {x1,y1,z1} and is done along direction pointed by vector {nsx,nsy,nsz}; the transverse matrices of the kick values are computed for the planes located at distances {ds1,ds2,ds3,...} from {x1,y1,z1}; nps is total number of points for longitudinal integration; one direction of the transverse grid is pointed by vector {n1x,n1y,n1z}, the other transverse direction is given by vector product of {n1x,n1y,n1z} and

{nsx,nsy,nsz}; r1 and r2 are ranges of the transverse grid, np1 and np2 are corresponding numbers of points; com is arbitrary string comment; d1 and d2 are steps of transverse differentiation (by default equal to the steps of the transverse grid). Returns list containing: [[1]]- list of triplets of 2D matrices representing kick values in the first and second transverse directions and the longitudinally-integrated squared transverse magnetic field, including the total matrices computed for whole range of longitudinal position and partial matrices corresponding to given longitudinal positions, [[2]],[[3]]- lists of positions defining the transverse grid, [[4]]- formatted string containing all the computed results (for saving into a text file).

?radFldFocKickPer

radFldFocKickPer[obj,{x1,y1,z1},{nsx,nsy,nsz},per,nper,{n1x,n1y,n1z}, r1,np1,r2,np2,com:"",{nh:1,nps:8,d1:0,d2:0}]

Computes matrices of 2nd order kicks of trajectory of relativistic charged particle in periodic magnetic field produced by the object obj. The longitudinal integration along one period starts at point {x1,y1,z1} and is done along direction pointed by vector {nsx,nsy,nsz}; per is period length, nper is number of full periods; one direction of the transverse grid is pointed by vector {n1x,n1y,n1z}, the other transverse direction is given by vector product of {n1x,n1y,n1z} and {nsx,nsy,nsz}; r1 and r2 are ranges of the transverse grid, np1 and np2 are corresponding numbers of points; com is arbitrary string comment; nh is maximum number of magnetic field harmonics to treat (default 1), nps is number of longitudinal points (default 8), d1 and d2 are steps of transverse differentiation (by default equal to the steps of the transverse grid). Returns list containing: [[1]]- matrix of kick values in the first transverse direction, [[2]]- matrix of kick values in the second transverse direction, [[3]]- matrix of longitudinally-integrated squared transverse magnetic field calculated on same transverse mesh as kicks, [[4]],[[5]]- lists of positions defining the transverse grid, [[6]]- formatted string containing the computed results (for saving into a text file).

The production of kickmaps using these functions is made more complicated by the RADIA coordinate system, which is shown in Figure 4.1 with the coordinate system that we used to derive our kickmap equations. In order

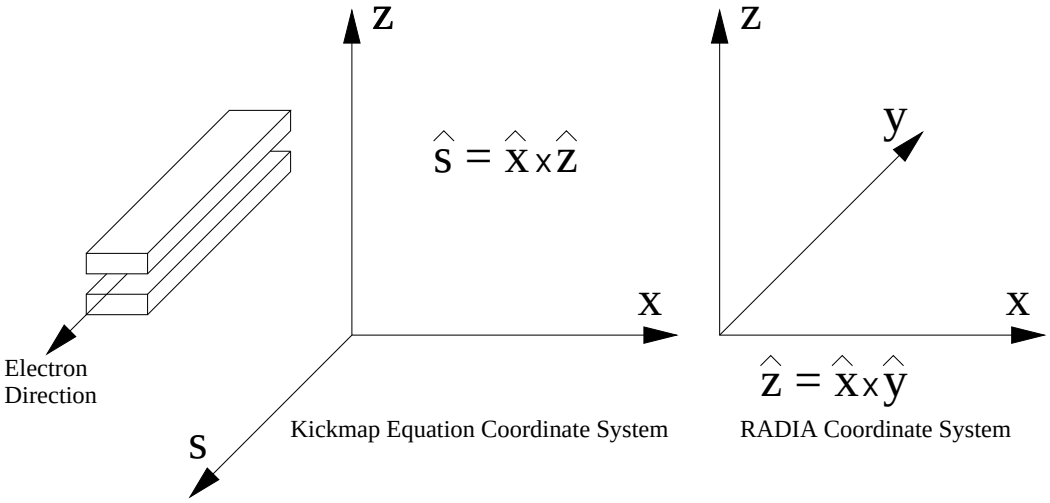

Figure 4.1: RADIA coordinate system

for us to maintain $+\hat{z}$ as up and $+\hat{x}$ as outboard, we are forced to have the electrons travel in the $-\hat{y}$ direction in RADIA coordinates.

This becomes important when we calculate kickmaps. In calculating kickmaps, our transverse coordinates are determined by $\{n1x, n1y, n1z\}$ and $\{n1x, n1y, n1z\} \times \{nsx, nsy, nsz\}$. In order to produce kickmaps with the correct axes, we want the first axis to be $\hat{x}$ so we take $\{n1x, n1y, n1z\} = \{1, 0, 0\}$. However, in order to make the second axis the vertical axis, we must take $\{nsx, nsy, nsz\} = \{0, 1, 0\}$ so that $\{n1x, n1y, n1z\} \times \{nsx, nsy, nsz\} =$

$\{0, 0, 1\}$ Since we have set $\{nsx, nsy, nsz\} = \{0, 1, 0\}$, this implies that the kickmap will be created by integrating through the device in the opposite direction as the electrons travel. However, our results of Section 4.1 tell us that we will get the same answer, so we need not worry. Switching $\{nsx, nsy, nsz\}$ to $\{0, -1, 0\}$ will cause the z axis to be inverted. This will cause problems with calculating the coupling terms of the kickmap unless very close attention is paid to the coordinate system.

Another important option to set is the starting location of the integration. For the periodic function, it is usually best to start one period from the center, $\{x1, y1, z1\} = \{0, -\text{Period}/2, 0\}$. For the full device function, it is best to start far enough from the device that the magnetic field is zero. It is also important to input the correct number of periods and period length when using the periodic function. Parameters such as grid size and spacing will vary from problem to problem. The number of longitudinal points used in the integration of the periodic function is by default 8, but more points may be desired for some problems. This will increase the time it takes to calculate a kickmap.

The sixth return value of radFldFocKickPer can be output to a file for inclusion into other programs. The following example was used to calculate the kickmaps for an undulator and output them to a file.

```
KickMapPer = radFldFocKickPer[ID,{0,-Period/2,0},{0,1,0},Period,Floor[nFull/2],
     {1,0,0},60,121,10,41,"Periodic Kickmap",{1,12,0,0}];
Export[NotebookDirectory[]<>"KickMapPeriodic.txt",KickMapPer[[6]]];
```

Since RADIA does not know the energy of the electron beam, it does not output $\Delta x'$ and $\Delta z'$ directly. Rather, it outputs $\Delta x'/\alpha^2$ and $\Delta z'/\alpha^2$, which have units T^2m^2. The output of RADIA depends only on the magnetic field of the insertion device. The RADIA output is completely machine dependent and can be imported into a simulation of any lattice with any electron beam energy.

Now that we are able to calculate kickmaps using RADIA, we can import them into a charged particle transport code such as elegant.

4.3 Importing Kickmaps into elegant

The charged particle transport code elegant [4] is used at the CLS in order to simulate beam dynamics. We can import a kickmap into elegant in order to simulate the effects of an insertion device on the electron beam. After a kickmap has been created by RADIA, the script `km2sdds` can be used to convert the RADIA output directly into an SDDS file, which is the format for elegant input files. Once the kickmap has been converted to SDDS format, it can be included in an elegant lattice by using the UKICKMAP element. The most important options for UKICKMAP are L and INPUT_FILE, which are the length of the insertion device in meters and the SDDS file where the kickmap is stored. Another useful factor is N_KICKS which specifies how many thin lens elements to use. Often, N_KICKS = 1 is sufficient. However, for longer devices, over which the beta functions vary, N_KICKS > 1 may be required. Other options exist, but they are not necessary for the basic use of the kickmap in tracking and linear optics calculations.

Using the kickmap to link the 3D magnetostatics code RADIA with the charged particle transport code elegant is a powerful technique. It is very useful in the design of insertion devices and in determining what correction, if any, will be needed to the linear and non-linear optics.

5 Kickmaps and Planar Insertion Devices

5.1 Vertical Focusing of an Ideal Insertion Device

Even an ideal planer insertion device has an effect on electron beam dynamics. Such a device will cause a vertical focusing of the beam. We derive this focusing effect from the kickmap equations.

Let us consider an ideal model of a planar insertion device. Such a device has a sinusoidal field which does not vary horizontally. However, Maxwell's equations require there to be a vertical field gradient. The transverse magnetic field for an ideal planar insertion device is therefore

$$\begin{aligned} B_x &= 0 \\ B_z &= B_0 \cos(k_p s) \cosh(k_p z) \end{aligned} \tag{5.1}$$

where $k_p \equiv 2\pi/\lambda_p$ and λ_p is the period length of the device [5]. The kickmap potential for this device is

$$\Phi = \frac{B_0^2}{k_p^2} \sin^2(k_p s) \cosh^2(k_p z) \tag{5.2}$$

which has transverse derivatives

$$\frac{\partial \Phi}{\partial x} = 0 \text{ and } \frac{\partial \Phi}{\partial z} = \frac{1}{k_p} \sinh(2k_p z) \sin^2(k_p s). \tag{5.3}$$

The horizontal kick is zero, $\Delta x' = 0$, and the vertical kick is given by

$$\begin{aligned} \Delta z' &= -\frac{\alpha^2 B_0^2}{2k_p} \sinh(2k_p z) \int_{-\infty}^{\infty} \sin^2(k_p s) ds \\ &= -\frac{\alpha^2 B_0^2 L}{4k_p} \sinh(2k_p z) \end{aligned} \tag{5.4}$$

where L is the length of the device and we recall that the integration limits $-\infty$ to ∞ are a mnemonic to represent integration over the entire, periodic insertion device. We can use the Taylor series expansion $\sinh(2k_p z) = 2k_p z + \ldots$ to obtain

$$\Delta z' = -\frac{\alpha^2 B_0^2 L}{2} z. \tag{5.5}$$

The sign of equation 5.5 describes a vertical focusing effect caused by the ideal insertion device. The strength depends on the amplitude of the device's magnetic field squared and linearly on its length. It is important to note that the focusing strength does not depend on the device's period.

We have shown that even an ideal, planar insertion device has a dynamic focusing effect. Such an insertion device must have infinitely wide poles. Now we will look at the effect of a planar insertion with finite width poles, which necessitates a field roll-off in the horizontal direction.

5.2 Field Roll-Off

While we would like every planar insertion device to have poles wide enough that they are effectively infinite, it is not practical. Large magnetic forces in planar insertion devices demand that pole widths be minimized. On the other hand, pole widths that are too narrow create problems with beam dynamics, as we will see in this section. The most famous case of insufficient pole width is the SPEAR BL11 wiggler [6]. This device was built with insufficient pole width and it caused a severe reduction of dynamic aperture. Even though the device was fixed by adding specially designed magnets to each end, the need to consider field roll-off in the design of planar insertion devices is critical.

We begin by extending our work for ideal, planar devices to devices with field roll off. We now let B_0 be a function of the horizontal positing giving us

$$B_z = B_0(x) \cos(k_p s) \cosh(k_p z) \tag{5.6}$$

Maxwell's equations require the curl of the magnetic field to be zero in free space so

$$\frac{\partial B_x}{\partial z} = \frac{\partial B_z}{\partial x} \tag{5.7}$$

which implies that

$$B_x = \frac{1}{k_p} B_0'(x) \cos(k_p s) \sinh(k_p z) \tag{5.8}$$

where $B_0'(x) = dB_0(x)/dx$. The kickmap potential is then

$$\Phi = \frac{1}{k_p^2} \left[\frac{B_0'^2(x)}{k_p^2} \sinh^2(k_p z) + B_0^2(x) \cosh^2(k_p z) \right] \sin^2(k_p s). \tag{5.9}$$

The horizontal kickmap is then

$$\Delta x' = -\frac{\alpha^2 L B_0'(x)}{2k_p^2} \left[\frac{B_0''(x)}{k_p^2} \sinh^2(k_p z) + B_0(x) \cosh^2(k_p z) \right]. \tag{5.10}$$

For small z we can use the approximation that $\sinh(k_p z) \simeq k_p z$ and $\cosh(k_p z) \simeq 1$ to obtain

$$\Delta x' = -\frac{\alpha^2 L B_0'(x)}{2k_p^2} \left[B_0''(x) z^2 + B_0(x) \right]. \tag{5.11}$$

When the field roll-off is small and z is small, we can write

$$\Delta x' = -\frac{\alpha^2 \lambda_p^2 L}{8\pi} B_0'(x) B_0(x) \tag{5.12}$$

where λ_p is the period of the insertion device. As in the case of vertical focusing by an ideal device, the horizontal focusing due to field roll-off is linearly proportional to the length of the device. However, the dependence on magnetic field is more complex because the kickmap is proportional to the magnetic field times its derivative. Only in the case of linear field roll-off would the kickmap reduce to simple linear focusing. We also see that the kickmap is proportional to the insertion device period squared, which again differs from the vertical focusing of an ideal planar device. For long-period wigglers, we expect field roll-off to be more of a problem than for short-period undulators.

They symmetry of $B_0(x)$ also has important consequences for the kickmap. Because planar devices have horizontal symmetry, $B_0(x)$ is an even function which implies that $B_0'(x)$ is an odd function. Therefore, we expect $\Delta x'$ to be an odd function. This implies that $\Delta x'(0,0) = 0$; in other words, the kickmap does not steer the stored beam and can only have odd multipole-like terms such as quadrupole, octupole and dodecapole[5].

We also note that $B_0(x)$ typically has a maximum at $x = 0$ and the field will roll-off and decrease the further one moves outward from the center of the device. This implies that $\Delta x' < 0$ when $x < 0$ and $\Delta x' > 0$ when $x > 0$. Field roll-off typically generates a horizontal defocusing of the electron beam.

We have seen that, for a planar insertion device, there will always be a vertical focusing effect due to the kickmap. Due to the finite pole width, there will be a horizontal defocusing effect. During the design of a device, the kickmaps must be calculated and simulations must be performed to determine if the effects are manageable.

5.3 Example Planar Insertion Device Kickmaps

In this section, we look at an example kickmap for a planar insertion device. The example device is the BioXAS wiggler which has 22 poles (including two half-poles) and a period length of ($\lambda_p = 150$ cm). A half-length RADIA model of the BioXAS wiggler is shown in Figure 5.1. The kickmaps calculated by RADIA for the wiggler are shown in Figure 5.2. The kickmaps are given in energy-independent units of T^2m^2. We can note a few interesting features of this kickmaps that relate to the calculations performed in this section.

First, pay careful attention to the x and z axis for the two kickmap plots as they are different; if we tried to plot them with the same axes, one plot would be difficult to see.

[5] The kickmap does not obey the multipole expansion and cannot generate true multipole terms. However, when we look only at the $z = 0$ plain, it can have terms proportional to x, x^3, x^5, etc. which we describe as being multipole-like.

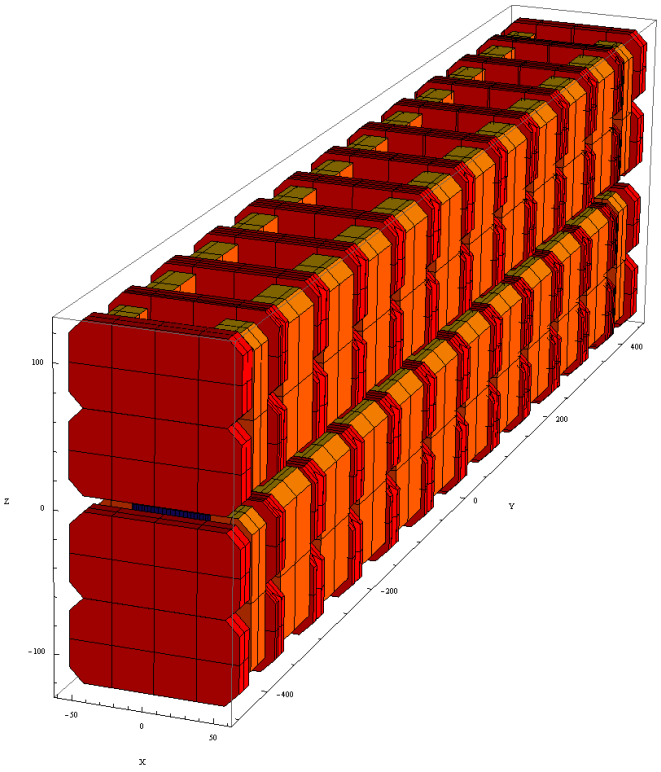

Figure 5.1: Half-length RADIA model of the BioXAS wiggler

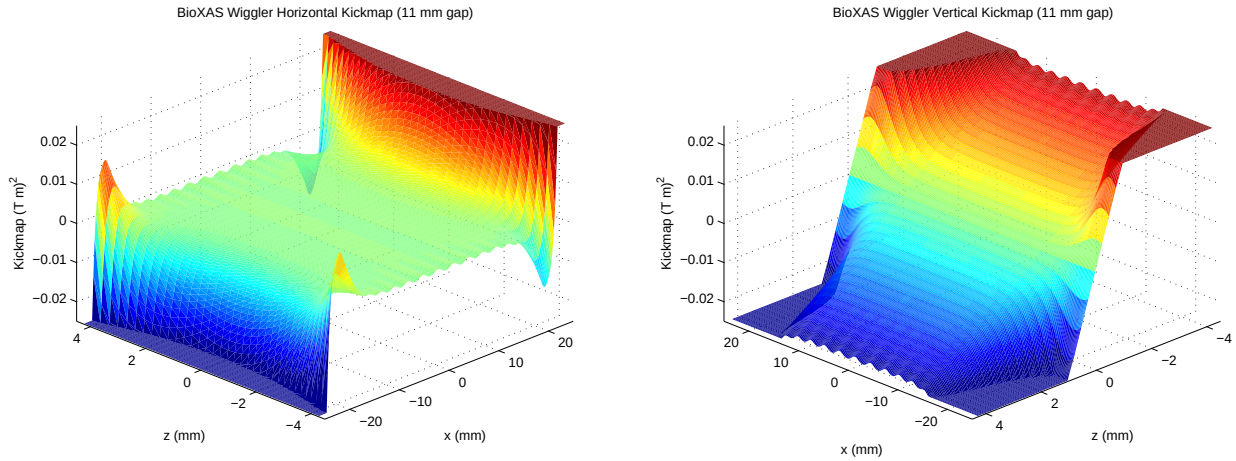

Figure 5.2: Horizontal kickmap $\Delta x'/\alpha^2$ (left) and vertical kickmap $\Delta z'/\alpha^2$ for the BioXAS wiggler $(\lambda_p = 150\,\text{cm})$

Note the horizontal kickmap. We observe the effects of field roll-off at $x = \pm 20$ mm. The good field region of this device is defined such that the electron beam will not be affected by the field-roll off as long as it is within 20 mm of the center. Should the beam be at 20 mm, the field roll-off will not matter as the limiting horizontal aperture at CLS is less than 20 mm.

Now note the vertical kickmap. At $x = \pm 20$ mm we observe the effect of field roll-off on the vertical kickmap as well as the horizontal. This effect could be calculated using the techniques of Section 5.2. We also note the linear focusing effect of the vertical kickmap in the good-field region. This is what gives the vertical kickmap its ramp-like feature.

Inside of the good field region -20 mm $< x < 20$ mm the horizontal kickmap is flat and the vertical kickmap is a linear function of the vertical position. The BioXAS wiggler resembles an ideal, planar insertion device in the good-field region.

6 Kickmaps and Elliptically Polarizing Undulators

6.1 Introduction to EPU Phase

Planar undulators and wigglers are useful for the production of intense beams of synchrotron radiation. However, they are limited to producing mainly linearly polarized photons. There is a scientific need to produce circularly polarized photons, and the elliptically polarizing undulator (EPU) was designed to meet this need. All of the EPUs in service or planned for CLS are of the APPLE II design [7]. A RADIA model of an APPLE II device with period $\lambda_p = 180$ mm is shown in Figure 6.1. Note the four girders: two on the top and two on the bottom. These

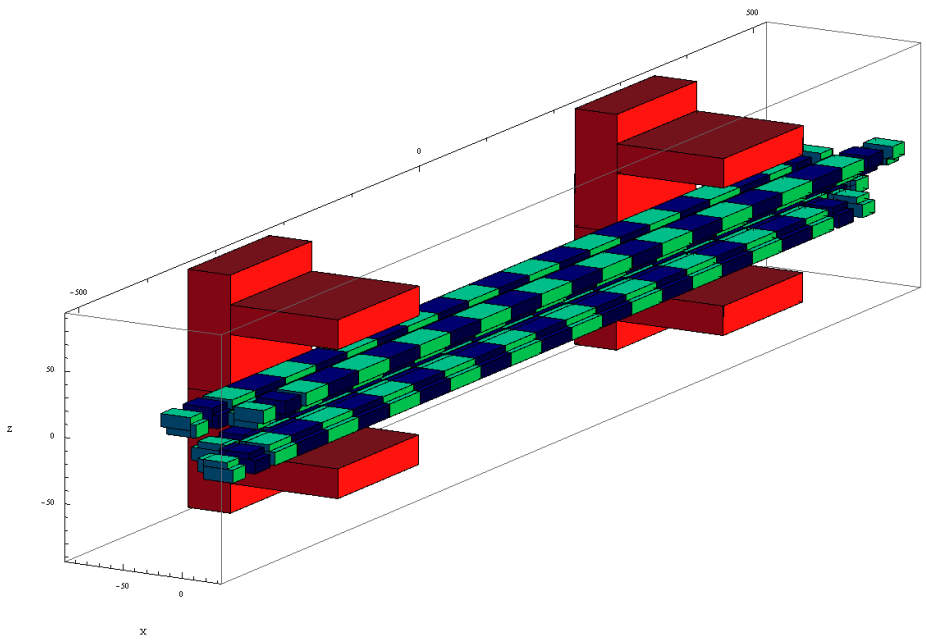

Figure 6.1: RADIA model of an EPU

girders can be moved independently of each other in order to produce radiation with variable polarization. If we move two diagonal girders in the same direction, the light output will be elliptical. If we move two diagonal girders in the opposite direction, the light output will be linear with an adjustable inclination angle. We can see that the EPU in Figure 6.1 will be producing elliptically polarized light.

Figure 6.2 shows the convention for girder numbering used at CLS. Each girder is numbered for its quadrant in the x-z plane. By adjusting the girders independently, we can generate beams of different polarizations. For

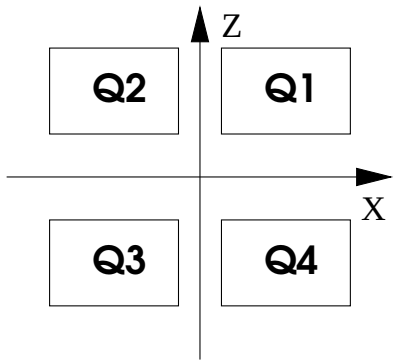

Figure 6.2: CLS girder numbering convention for an EPU

planar insertion devices we have only one degree of freedom: the gap size. When discussing EPUs, we have four degrees of freedom: one for the gap size and three for the girder positions. Since it's the relative girder positions that matter, we have three degrees of freedom for four girders.

Let Q_1, Q_2, Q_3 and Q_4 be the four girder positions. We will define three phases which will exhaust our degrees of freedom: the elliptical phase, ϕ_E, the linear phase with positive inclination, ϕ_L^+, and the linear phase with negative inclination, ϕ_L^-. We relate these two sets of variables by

$$\begin{aligned} Q_1 &= \frac{1}{2}\phi_E + \phi_L^+ \\ Q_2 &= -\frac{1}{2}\phi_E + \phi_L^- \\ Q_3 &= \frac{1}{2}\phi_E - \phi_L^+ \\ Q_4 &= -\frac{1}{2}\phi_E - \phi_L^- \end{aligned} \tag{6.1}$$

If we set $\phi_E = \phi_L^- = \phi_L^+ = 0$ the EPU will produce horizontally polarized photons and the analysis will reduce to that of the planar device. However, the field roll-off is made more complex due to the gap between girders.

An EPU with only ϕ_E non-zero will produce elliptically polarized photons. The eccentricity of the ellipse is controlled by the magnitude of ϕ_E and the helicity of the photons is controlled by the sign of ϕ_E. The elliptical phase $\phi_E = \pm\lambda_p/4$ is called elliptical quarter phase and will produce photons which are very near to being circular[6]. Another important phase is $\phi_E = \pm\lambda_p/2$, which corresponds to vertically polarized photons. It is interesting to note that with only the elliptical phase degree of freedom, an EPU can produce horizontal, vertically and elliptically polarized light. This is sufficient for many scientific programs.

For some programs, linearly polarized photons with an inclination angle other than 0 (horizontal) and $\pm\pi/2$ (vertical) are required. These EPUs will also need the linear inclined degrees of freedom. For the moment, we will not mix degrees of freedom so we will assume that $\phi_E = 0$ and that only one of ϕ_L^+ and ϕ_L^- are non-zero at any time. It is intuitive, but incorrect, that the angle of inclination of the polarization vector will switch quadrants when ϕ_L^+ or ϕ_L^- switches sign. Instead, the angle of inclination for $\phi_L^+ \neq 0$ will always be positive as the angle of inclination for $\phi_L^- \neq 0$ will always be negative. Switching the sign of ϕ_L^+ or ϕ_L^- has no effect on the sign of the angle of inclination. A commonly discussed inclined phase is $\phi_L^+ = \pm\lambda_p/4$ or $\phi_L^- = \pm\lambda_p/4$, which we refer to as linear quarter phase. This is close to, but not quite, an inclination of $\pm\pi/4$.

For applications with photon energies less than 100 eV, beamline optics can distort circularly polarized light into an ellipse with an inclination. Beamline scientists can compensate for this by altering the polarization ellipse

[6]Eccentricity also has some gap dependence so the phase of perfectly circular photons is not the same for all gaps, but is always near elliptical quarter phase.

emitted by the EPU. This requires mixing the elliptical phase ϕ_E and one of the linear phases, ϕ_L^+ or ϕ_L^- to produce a polarization with a given eccentricity and inclination at the EPU source. This mode of operation has been given the name 'Universal Mode'. At the time of writing, the only APPLE II EPU that we are aware of which operates in universal mode is UE112 at BESSY [8].

Universal mode requires three degrees of freedom. Let us define the composite linear phase ϕ_L^c such that

$$\left.\begin{array}{rl} \phi_L^+ = & |\phi_L^c| \\ \phi_L^- = & 0 \end{array}\right\} \text{ if } 0 < \phi_L^c$$
$$\left.\begin{array}{rl} \phi_L^+ = & 0 \\ \phi_L^- = & |\phi_L^c| \end{array}\right\} \text{ if } \phi_L^c < 0 \tag{6.2}$$

Then our three degrees of freedom are the gap, ϕ_E and ϕ_L^c. There exists a non-linear mapping of these degrees of freedom into the eccentricity and inclination of the polarization ellipse and the photon energy [8].

There remains some question about what happens if we mix ϕ_L^+ and ϕ_L^-. This will have the effect of changing the energy of the photons, a task that we now accomplish by changing the gap. In fact, the Swiss Light Source has developed an APPLE II EPU with fixed gap. Their UE44 device uses only girder shifts to adjust photon energy [9].

For the purpose of this document, we will assume that the EPU has a gap drive for energy adjustment. As such, we will assume that only one of ϕ_L^+ or ϕ_L^- will be non-zero at any time. This will permit our APPLE II to operate in universal mode, similar to UE112 at BESSY.

APPLE II devices have a complex magnetic field structure and numerical methods are needed to calculate kickmaps. Some features of these kickmaps can be calculated by symmetry considerations. We are interested in determining when to expect terms that couple the transverse coordinates. In other words, when does $\Delta x'$ depend on z or $\Delta z'$ depend on x. We are also interested in the symmetries of the kickmaps. If $\Delta x'$ and $\Delta z'$ are odd functions, then they will be zero at $(x, z) = (0, 0)$ and will not steer the stored beam.

The symmetries in the following sections were first determined using numerical methods. Knowing the numerical solutions greatly simplified building the analytical arguments presented here. The reader is encouraged to verify the following results by comparing the fields and kickmaps generated by a RADIA model of an EPU. Example kickmaps will be presented as we progress through the next sections.

6.2 Symmetries of the EPU Magnetic Field

We will begin our discussion by looking at the symmetries of the magnetic field of an EPU. We will start with the simplest possible polarization setting, horizontal, where all phases are set to zero and the magnetic field is purely vertical, up-to fringing effects. Figure 6.3 shows a cross section of the EPU in horizontal polarization

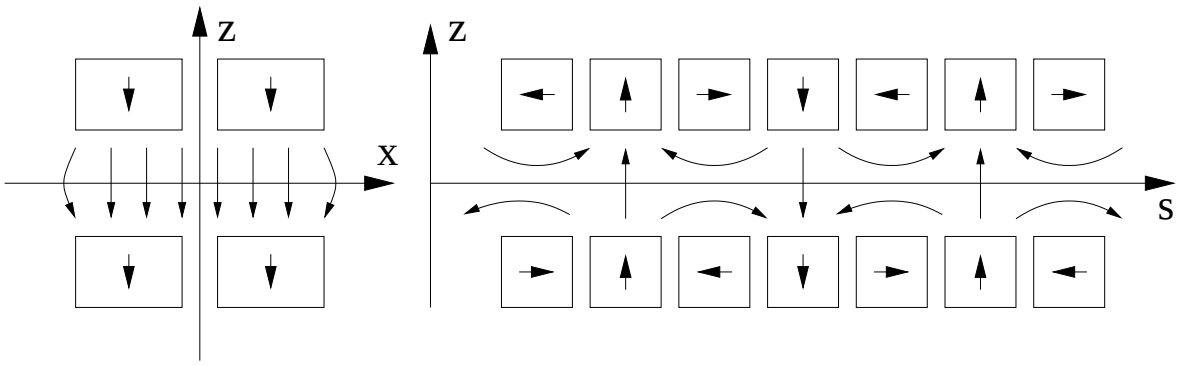

Figure 6.3: Vertical magnetic field for an EPU in horizontal polarization mode

mode. We note that the device is symmetric about the horizontal component so we can write

$$\begin{aligned} B_x(-x,z,s) &= -B_x(x,z,s) \\ B_z(-x,z,s) &= +B_z(x,z,s) \\ B_s(-x,z,s) &= +B_s(x,z,s). \end{aligned} \tag{6.3}$$

Unlike a planar insertion device, an APPLE II EPU must have an integer number of periods so we have a similar symmetry about the longitudinal coordinate

$$\begin{aligned} B_x(x,z,-s) &= +B_x(x,z,s) \\ B_z(x,z,-s) &= +B_z(x,z,s) \\ B_s(x,z,-s) &= -B_s(x,z,s). \end{aligned} \tag{6.4}$$

The device is asymmetric about the vertical coordinate so we write

$$\begin{aligned} B_x(x,-z,s) &= -B_x(x,z,s) \\ B_z(x,-z,s) &= +B_z(x,z,s) \\ B_s(x,-z,s) &= -B_s(x,z,s). \end{aligned} \tag{6.5}$$

We use the symmetries of equations 6.3, 6.4 and 6.5 to derive additional symmetries. We will refer to the equations 6.6, 6.7 and 6.8 as the elliptical symmetries, for reasons that will be explained soon. For x and z,

$$\begin{aligned} B_x(-x,-z,s) &= +B_x(x,z,s) \\ B_z(-x,-z,s) &= +B_z(x,z,s) \\ B_s(-x,-z,s) &= -B_s(x,z,s) \end{aligned} \tag{6.6}$$

for x and s,

$$\begin{aligned} B_x(-x,z,-s) &= -B_x(x,z,s) \\ B_z(-x,z,-s) &= +B_z(x,z,s) \\ B_s(-x,z,-s) &= -B_s(x,z,s) \end{aligned} \tag{6.7}$$

and for z and s,

$$\begin{aligned} B_x(x,-z,-s) &= -B_x(x,z,s) \\ B_z(x,-z,-s) &= +B_z(x,z,s) \\ B_s(x,-z,-s) &= +B_s(x,z,s). \end{aligned} \tag{6.8}$$

We will refer to equation 6.9 as the linear incline symmetry, again for reasons that will be explained shortly,

$$\begin{aligned} B_x(-x,-z,-s) &= +B_x(x,z,s) \\ B_z(-x,-z,-s) &= +B_z(x,z,s) \\ B_s(-x,-z,-s) &= +B_s(x,z,s). \end{aligned} \tag{6.9}$$

Previously we have discussed operating the EPU in elliptical mode, where only ϕ_E is non-zero, in linear inclined mode where only one of ϕ_L^+ or ϕ_L^- is non-zero, and in universal mode which mixes elliptical and linear incline modes. It is important to note that the horizontal mode is the only mode that is both elliptical and linear incline[7]. Therefore, any symmetries of the elliptical and linear incline modes must be present in the horizontal mode. The converse of this statement is not true. When the girders are moved, symmetry is broken and the number of symmetries can decrease, or all symmetry can be eliminated altogether.

The basic symmetries obtained from reflecting the device about one coordinate, given in equations 6.3, 6.4 and 6.5, no longer exist in the elliptical or linear incline modes. In the elliptical mode, we see from Figure 6.4,

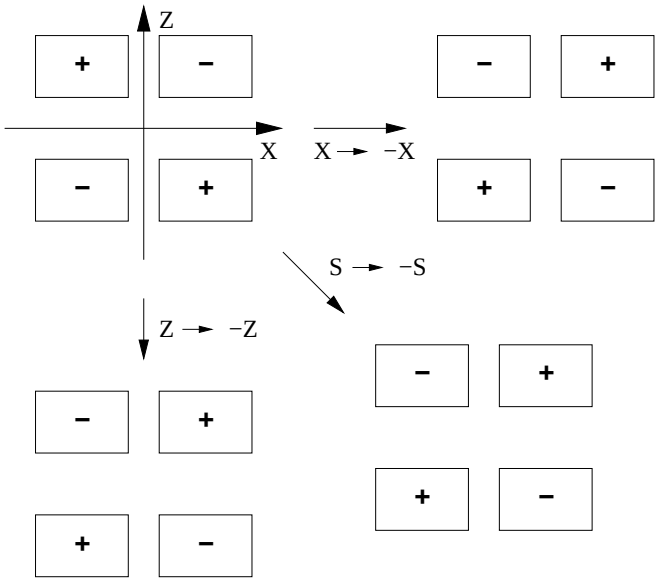

Figure 6.4: Effect of mirroring elliptical mode by the three coordinates

that mirroring two coordinates will return the device to a configuration similar to its original. Because of the asymmetry in the vertical field, determining $+$ and $-$ signs for the fields can be difficult for the simple picture given by Figure 6.4. Fortunately, this picture shows that the elliptical symmetries of equations 6.6, 6.7 and 6.8 continue to hold. Note that a third mirroring of the device would not return us to the original, so the linear incline symmetry does not hold for elliptical mode.

In considering the linear incline symmetry, we will consider only the positive inclination angle case, with $-\lambda_p/2 \leq \phi_L^+ \leq \lambda_p/2$ and $\phi_L^- = 0$, with the understanding that the negative inclination case works exactly the same. Figure 6.5 shows the symmetry of the linear incline mode with $\phi_L^+ > 0$, which implies that girder Q_1 is moved toward

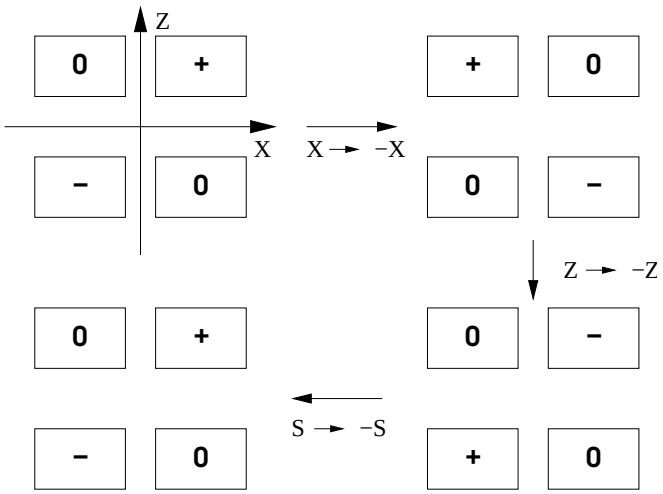

Figure 6.5: Symmetry of the linear incline mode

us, girder Q_3 is moved away from us and girders Q_2 and Q_4 remain unmoved. Unlike the elliptical mode, two reflections do not return the EPU to a symmetric configuration. Rather, all three reflections are required, and the

[7] Vertically polarized photons can be produced by either the elliptical or linear incline modes, but the phases ϕ_E, ϕ_L^+ and ϕ_L^- will be distinctly one mode or another.

linear incline modes obey the linear incline symmetry given by equation 6.9. The elliptical symmetries do not hold for the linear incline mode.

Since the linear incline symmetries do not hold for elliptical mode, and the elliptical symmetries do not hold for linear incline mode, none of these symmetries will hold for universal mode.

In this section, we have examined the symmetries of an EPU of APPLE II design. We began by noting all the symmetries for an EPU in horizontal polarization mode, which is the only mode that is both an elliptical mode and a linear incline mode. We see that the device and its magnetic fields undergo symmetry breaking when girders are moved from horizontal into other configuration of the elliptical and linear incline modes. In the elliptical mode, two reflections are required to regain symmetry, and the elliptical symmetries of equations 6.6, 6.7 and 6.8 continue to hold. In the linear incline modes, three reflections are required to regain symmetry, and the linear incline symmetry of equation 6.9 continues to hold. In universal mode, no symmetries hold.

6.3 Symmetries of Kickmaps for a Given EPU Phase

In Section 6.2 we found the symmetries of elliptical and linear incline modes. We can now use the symmetries of the magnetic fields to find symmetries of the kickmaps.

We begin by looking at the elliptical mode, which has symmetries given by equations 6.6, 6.7 and 6.8. The horizontal kickmap is given by

$$\Delta x'(x,z) = -\frac{\alpha^2}{2}\int_{-\infty}^{\infty}\frac{\partial}{\partial x}\left[\left(\int_{-\infty}^{s}B_x(x,z,s')ds'\right)^2+\left(\int_{-\infty}^{s}B_z(x,z,s')ds'\right)^2\right]ds. \tag{6.10}$$

We can use this equation to examine $\Delta x'$ under a vertical reflection,

$$\begin{aligned}\Delta x'(x,-z) &= -\frac{\alpha^2}{2}\int_{-\infty}^{\infty}\frac{\partial}{\partial x}\left[\left(\int_{-\infty}^{s}B_x(x,-z,s')ds'\right)^2+\left(\int_{-\infty}^{s}B_z(x,-z,s')ds'\right)^2\right]ds\\ &= -\frac{\alpha^2}{2}\int_{-\infty}^{\infty}\frac{\partial}{\partial x}\left[\left(\int_{-\infty}^{s}B_x(x,z,-s')ds'\right)^2+\left(\int_{-\infty}^{s}B_z(x,z,-s')ds'\right)^2\right]ds\\ &= \Delta x'(x,z)\end{aligned} \tag{6.11}$$

where we used the symmetry of equation 6.8 in the first step and the results of Section 4.1 in the second step. The horizontal reflection is similar, but slightly different

$$\begin{aligned}\Delta x'(-x,z) &= -\frac{\alpha^2}{2}\int_{-\infty}^{\infty}-\frac{\partial}{\partial x}\left[\left(\int_{-\infty}^{s}B_x(-x,z,s')ds'\right)^2+\left(\int_{-\infty}^{s}B_z(-x,z,s')ds'\right)^2\right]ds\\ &= +\frac{\alpha^2}{2}\int_{-\infty}^{\infty}\frac{\partial}{\partial x}\left[\left(\int_{-\infty}^{s}B_x(x,z,-s')ds'\right)^2+\left(\int_{-\infty}^{s}B_z(x,z,-s')ds'\right)^2\right]ds\\ &= -\Delta x'(x,z)\end{aligned} \tag{6.12}$$

where we used the chain rule of differentiation and the symmetry of equation 6.7 in the first step and the results of Section 4.1 in the second step. We see that $\Delta x'(x,z)$ is odd in x and even in z. Likewise, $\Delta z'(-x,z)=\Delta z'(x,z)$ and $\Delta z'(x,-z)=-\Delta z'(x,z)$, which means that the vertical kickmap is even in x and odd in z. In Figure 6.6 We plot an example kickmaps for the QMSC EPU180 currently under construction at CLS. It is easy to observe the odd/even behaviour of the kickmaps.

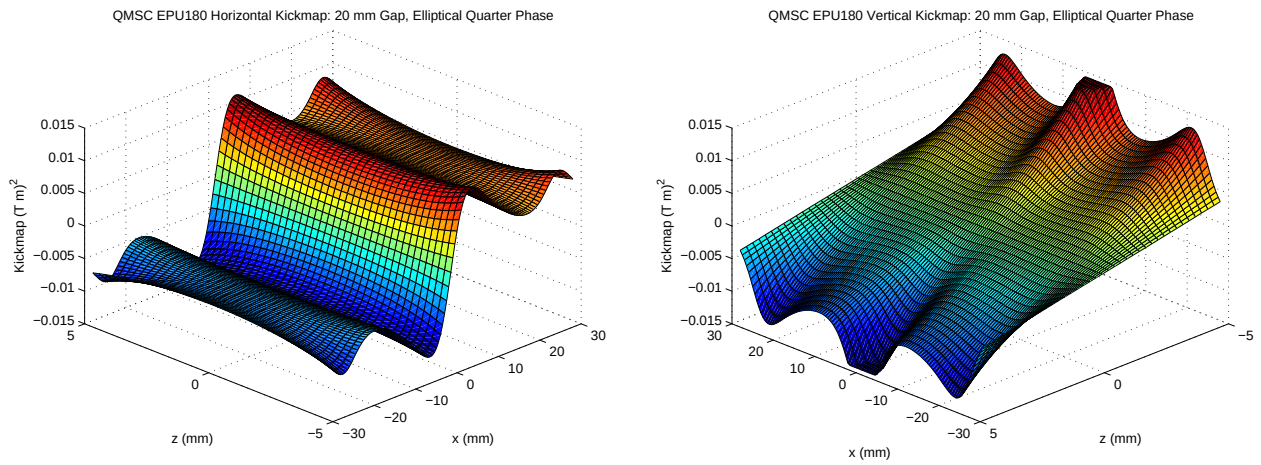

Figure 6.6: Horizontal kickmap $\Delta x'/\alpha^2$ (left) and vertical kickmap $\Delta z'/\alpha^2$ for the QMSC EPU180 in elliptical quarter phase at a gap of 20 mm

It is also worth noting that, for elliptical mode, $\Delta x'(0,z) = 0$ and $\Delta z'(x,0) = 0$ by the properties of odd functions. In other words, a particle on the vertical axis will not experience a horizontal kick and a particle on the horizontal axis will not experience a vertical kick. It is not an intuitive results, but the symmetry breaking required to operate an EPU in the elliptical mode does not cause transverse coupling of the stored beam.

The argument for the incline mode is similar, but the symmetry is slightly different. The symmetries found for the elliptical mode kickmaps do not apply, but we are able to derive the following symmetry

$$\begin{aligned}
\Delta x'(-x,-z) &= -\frac{\alpha^2}{2}\int_{-\infty}^{\infty} -\frac{\partial}{\partial x}\left[\left(\int_{-\infty}^{s} B_x(-x,-z,s')ds'\right)^2 + \left(\int_{-\infty}^{s} B_z(-x,-z,s')ds'\right)^2\right] ds \\
&= +\frac{\alpha^2}{2}\int_{-\infty}^{\infty} \frac{\partial}{\partial x}\left[\left(\int_{-\infty}^{s} B_x(x,z,-s')ds'\right)^2 + \left(\int_{-\infty}^{s} B_z(x,z,-s')ds'\right)^2\right] ds \\
&= -\Delta x'(x,z)
\end{aligned} \tag{6.13}$$

where we used the chain rule of differentiation and the symmetry of equation 6.9 in the first step and the results of Section 4.1 in the second step. Likewise, $\Delta z'(-x,-z) = -\Delta z'(x,z)$. We note that equations 6.11 and 6.12 together imply the symmetry $\Delta x'(-x,-z) = -\Delta x'(x,z)$ also applies to the elliptical mode, but the converse it not true. In Figure 6.7 We plot an example kickmaps for the QMSC EPU180 currently under construction at CLS. It is easy to observe the symmetry in the kickmap plots.

We also observe that, for elliptical and linear incline modes,

$$\begin{aligned}
\Delta z'(0,z) &\quad \text{is odd} \\
\Delta z'(x,0) &\quad \text{is odd} \\
\Delta x'(0,z) &\quad \text{is odd} \\
\Delta x'(x,0) &\quad \text{is odd}
\end{aligned} \tag{6.14}$$

and

$$\Delta x'(0,0) = \Delta z'(0,0) = 0 \tag{6.15}$$

implies that we will get only odd multipole-like terms and that the kickmap does not steer the beam.

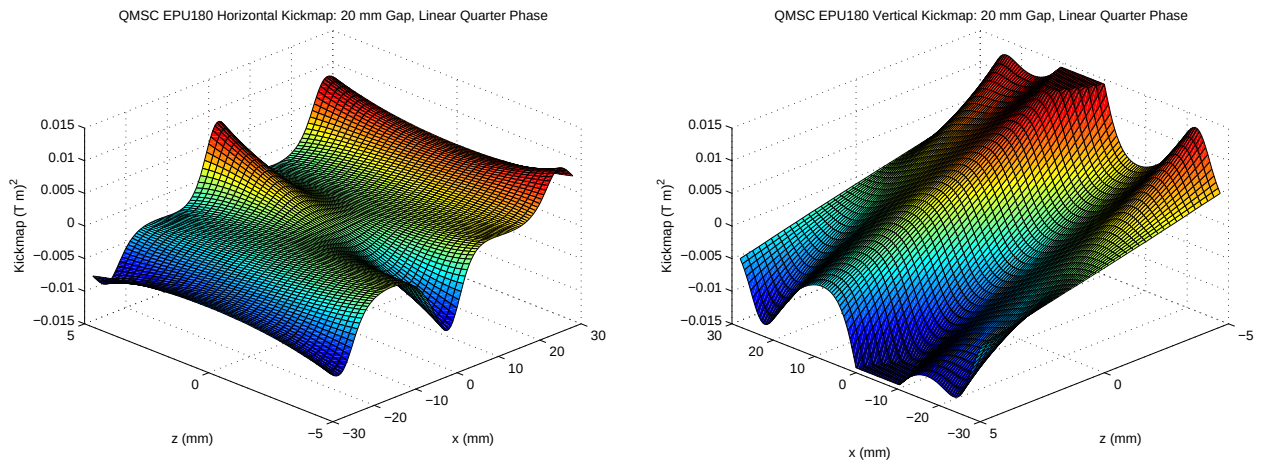

Figure 6.7: Horizontal kickmap $\Delta x'/\alpha^2$ (left) and vertical kickmap $\Delta z'/\alpha^2$ for the QMSC EPU180 in linear quarter phase at a gap of 20 mm

Unfortunately, there are no symmetries of the magnetic field for universal mode. We therefore are unable to calculate any symmetries of the kickmaps. Universal mode can generate even multipole-like terms and steer the beam.

For completeness, the kickmaps for the horizontal and vertical polarization modes of the EPU are shown Figure 6.8. The elliptical mode symmetries are apparent.

In conclusion, we have found symmetries in the kickmaps for the elliptical and linear incline modes. However, we were not able to find any symmetries for the universal mode. In both the linear incline and elliptical modes,

$$\begin{aligned} \Delta x'(-x,-z) &= -\Delta x'(x,z) \\ \Delta z'(-x,-z) &= -\Delta z'(x,z). \end{aligned} \tag{6.16}$$

This has the important consequence that, along the $x = 0$ or $z = 0$ axes, the horizontal and vertical kickmaps are both odd functions.

For the elliptical mode, the kickmaps have further symmetry that is not found in the linear incline modes:

$$\begin{aligned} \Delta x'(x,-z) &= \Delta x'(x,z) \\ \Delta x'(-x,z) &= -\Delta x'(x,z) \\ \Delta z'(x,-z) &= -\Delta z'(x,z) \\ \Delta z'(-x,z) &= \Delta z'(x,z). \end{aligned} \tag{6.17}$$

This has the important consequence that $\Delta x'(0,z) = \Delta z'(x,0) = 0$.

6.4 Transformations of the EPU Magnetic Field with Phase

In Section 6.2 we looked at the magnetic field symmetries for a fixed phase of the EPU. We then used those symmetries to derive symmetries of the EPU kickmaps for the elliptical and linear incline modes in Section 6.3.

We now look at the transformation of the magnetic fields and transformation of kickmaps under transformation of EPU phase. We will be primarily concerned with three transformations: $\phi_E \to -\phi_E$, $\phi_L^+ \to -\phi_L^+$ and $\phi_L^+ \to \phi_L^-$. For the following discussion, we assume that the EPU is in universal mode.

We begin our study of the three transformation by representing them graphically in Figures 6.9 and 6.10. In these figures, we begin with a representation of the EPU in universal mode with the left picture representing the

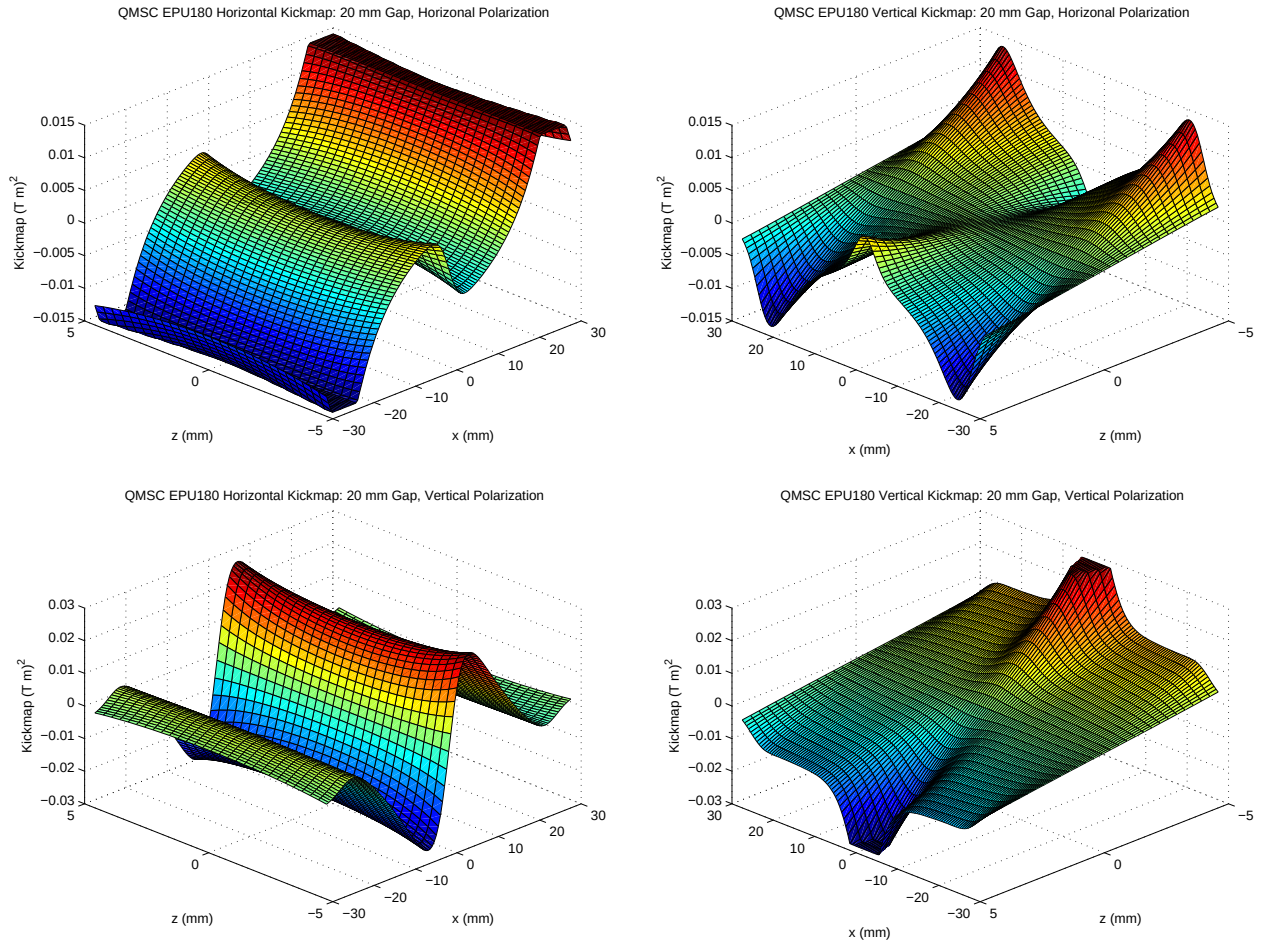

Figure 6.8: Horizontal kickmap $\Delta x'/\alpha^2$ (left) and vertical kickmap $\Delta z'/\alpha^2$ (right) for the QMSC EPU180 in horizontal mode (top) and vertical mode (bottom; different vertical scale) at a gap of 20 mm

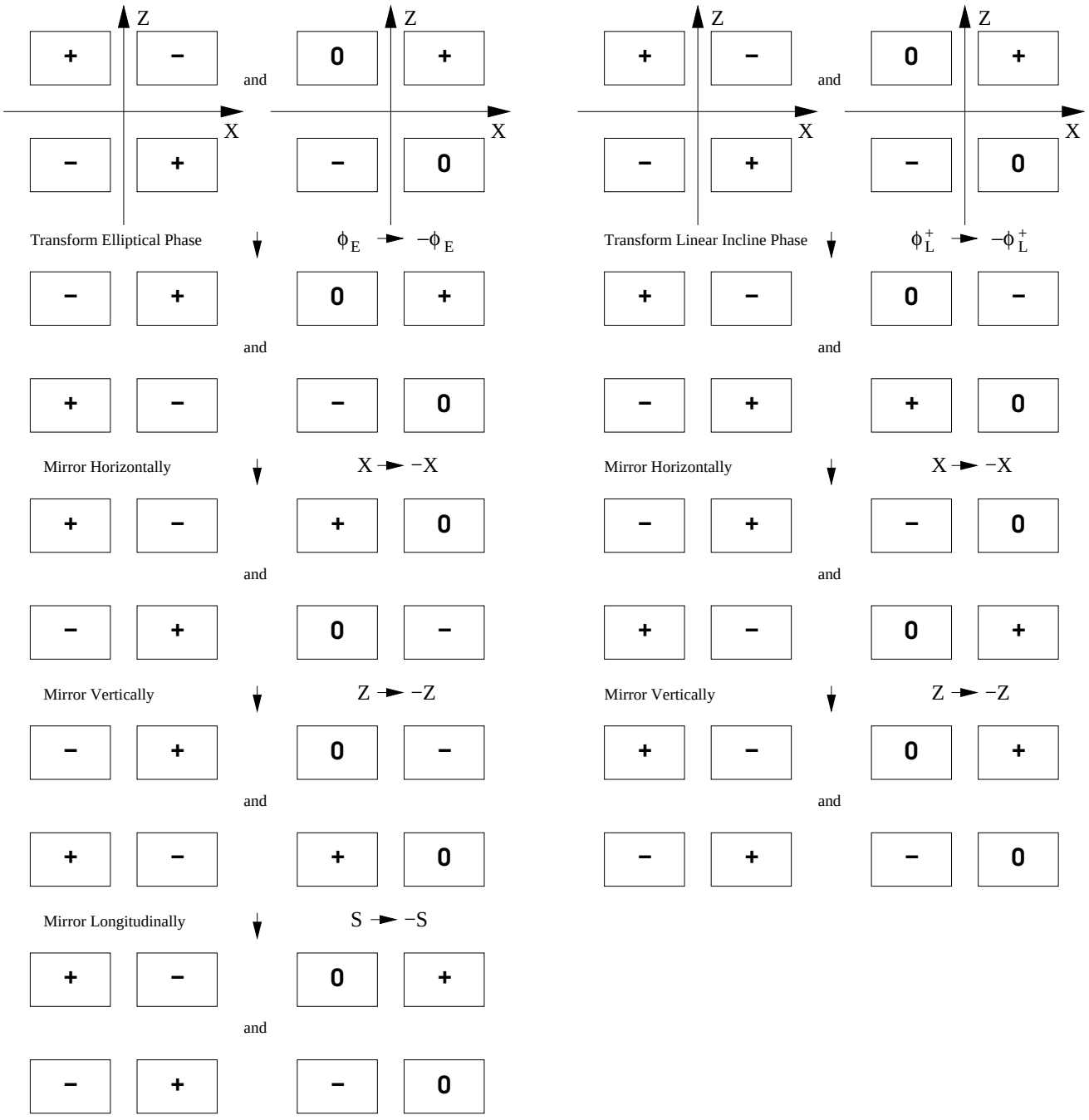

Figure 6.9: Reflections required to return a universal mode EPU configuration back to its original configuration after an elliptical or linear incline phase transformation, $\phi_E \rightarrow -\phi_E$ or $\phi_L^+ \rightarrow -\phi_L^+$ respectively.

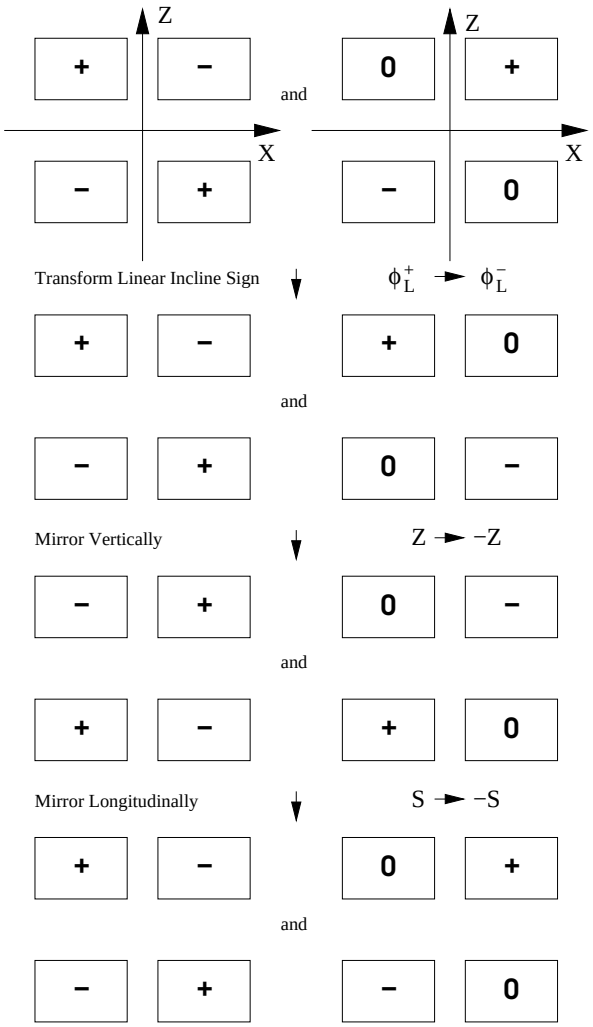

Figure 6.10: Reflections required to return a universal mode EPU configuration back to its original configuration after a linear incline sign transformation, $\phi_L^+ \rightarrow \phi_L^-$

elliptical phase and the right picture representing the linear incline phase. Our first step is to apply one of the transformations $\phi_E \to -\phi_E$, $\phi_L^+ \to -\phi_L^+$ or $\phi_L^+ \to \phi_L^-$. We then apply a series of reflections to return the EPU representations to their original configuration. In this way, we can calculate the effect of the transformation on the magnetic field. Taking into account the vertical asymmetry of the device, Figures 6.9 and 6.10 imply that

$$\begin{aligned} \phi_E &\to -\phi_E \text{ implies} \\ B_x(x,z,s) &\to +B_x(-x,-z,-s) \\ B_z(x,z,s) &\to +B_z(-x,-z,-s) \\ B_s(x,z,s) &\to +B_s(-x,-z,-s), \end{aligned} \tag{6.18}$$

$$\begin{aligned} \phi_L^+ &\to -\phi_L^+ \text{ implies} \\ B_x(x,z,s) &\to +B_x(-x,-z,s) \\ B_z(x,z,s) &\to +B_z(-x,-z,s) \\ B_s(x,z,s) &\to -B_s(-x,-z,s) \end{aligned} \tag{6.19}$$

and

$$\begin{aligned} \phi_L^+ &\to \phi_L^- \text{ implies} \\ B_x(x,z,s) &\to -B_x(x,-z,-s) \\ B_z(x,z,s) &\to +B_z(x,-z,-s) \\ B_s(x,z,s) &\to +B_s(x,-z,-s). \end{aligned} \tag{6.20}$$

One may wonder at how we found the signs of the magnetic fields in the transformations of equations 6.18, 6.19 and 6.20. In fact, we have already calculated these signs. While the horizontal polarization mode is special, it is still a configuration in universal mode. Therefore, any symmetry that exists for a transformation in universal mode exists for the horizontal mode as well, but the converse is not true. Under the three transformations $\phi_E \to -\phi_E$, $\phi_L^+ \to -\phi_L^+$ and $\phi_L^+ \to \phi_L^-$, the horizontal mode EPU transforms into itself. Therefore, the signs for equation 6.18 are given by equation 6.9, the signs for equation 6.19 are given by equation 6.6 and the sings for equation 6.20 are given by equation 6.8.

6.5 Transformations of the EPU Kickmaps with Phase

In Section 6.4 we calculated how the magnetic fields transform under the three transformations $\phi_E \to -\phi_E$, $\phi_L^+ \to -\phi_L^+$ and $\phi_L^+ \to \phi_L^-$. The results can be found in equations 6.18, 6.19 and 6.20. We will now use the transformations of the magnetic fields to calculate the transformations of the kickmaps.

For the elliptical phase transformation, $\phi_E \to -\phi_E$

$$\begin{aligned} \Delta x'(x,z) &\to -\frac{\alpha^2}{2}\int_{-\infty}^{\infty} -\frac{\partial}{\partial x}\left[\left(\int_{-\infty}^{s} B_x(-x,-z,-s')ds'\right)^2 + \left(\int_{-\infty}^{s} B_z(-x,-z,-s')ds'\right)^2\right] ds \\ &= +\frac{\alpha^2}{2}\int_{-\infty}^{\infty} \frac{\partial}{\partial x}\left[\left(\int_{-\infty}^{s} B_x(-x,-z,s')ds'\right)^2 + \left(\int_{-\infty}^{s} B_z(-x,-z,s')ds'\right)^2\right] ds \\ &= -\Delta x'(-x,-z) \end{aligned} \tag{6.21}$$

where we used the chain rule of differentiation and the transformation of equation 6.18 in the first step and the results of Section 4.1 in the second step. Likewise, $\Delta z'(x,z) \to -\Delta z'(-x,-z)$.

For the linear incline phase transformation, $\phi_L^+ \rightarrow -\phi_L^+$

$$\begin{aligned}\Delta x'(x,z) &\rightarrow -\frac{\alpha^2}{2}\int_{-\infty}^{\infty} -\frac{\partial}{\partial x}\left[\left(\int_{-\infty}^{s} B_x(-x,-z,s')ds'\right)^2 + \left(\int_{-\infty}^{s} B_z(-x,-z,s')ds'\right)^2\right]ds \\ &= -\Delta x'(-x,-z) \end{aligned} \tag{6.22}$$

where we used the chain rule of differentiation and the transformation of equation 6.19. Likewise, $\Delta z'(x,z) \rightarrow -\Delta z'(-x,-z)$.

For the inclination sign transformation, $\phi_L^+ \rightarrow \phi_L^-$

$$\begin{aligned}\Delta x'(x,z) &\rightarrow -\frac{\alpha^2}{2}\int_{-\infty}^{\infty} \frac{\partial}{\partial x}\left[\left(\int_{-\infty}^{s} B_x(x,-z,-s')ds'\right)^2 + \left(\int_{-\infty}^{s} B_z(x,-z,-s')ds'\right)^2\right]ds \\ &= \Delta x'(x,-z) \end{aligned} \tag{6.23}$$

where we used the transformation of equation 6.20 in the first step and the results of Section 4.1 in the second step. Likewise, $\Delta z'(x,z) \rightarrow -\Delta z'(x,-z)$ where the additional minus sign comes from the chain rule of differentiation. Note that the transformation of the magnetic fields and kickmaps for the inverse transformation, $\phi_L^- \rightarrow \phi_L^+$ is the same.

Using the results of equations 6.22 and 6.23, we find that the transformation for $\phi_L^- \rightarrow -\phi_L^-$ is the same as $\phi_L^+ \rightarrow -\phi_L^+$.

In conclusion, we have calculated the transformations of the kickmaps under the transformation of the elliptical and linear incline phases. We find that for the transformations $\phi_E \rightarrow -\phi_E$, $\phi_L^+ \rightarrow -\phi_L^+$ and $\phi_L^- \rightarrow -\phi_L^-$ the kickmaps undergo transformations $\Delta x'(x,z) \rightarrow -\Delta x'(-x,-z)$ and $\Delta z'(x,z) \rightarrow -\Delta z'(-x,-z)$. For the transformations $\phi_L^+ \rightarrow \phi_L^-$ and $\phi_L^- \rightarrow \phi_L^+$ the kickmaps undergo transformations $\Delta x'(x,z) \rightarrow \Delta x'(x,-z)$ and $\Delta z'(x,z) \rightarrow -\Delta z'(x,-z)$. These transformations can be seen in the example kickmaps of Figures 6.11 and 6.12.

There are some interesting special cases of these transformations. Let us consider a pure elliptical or pure linear incline modes, where only one phase, ϕ_E, ϕ_L^+ or ϕ_L^-, is non-zero. From equation 6.16, if we are in a pure elliptical mode or pure linear incline mode, the kickmaps have the symmetry $-\Delta x'(-x,-z) = \Delta x'(x,z)$ and $-\Delta z'(-x,-z) = \Delta z'(x,z)$. Therefore, if we are in a pure elliptical mode or pure linear incline mode, the kickmap will transform as $\Delta x'(x,z) \rightarrow \Delta x'(x,z)$ and $\Delta z'(x,z) \rightarrow \Delta z'(x,z)$ when $\phi_E \rightarrow -\phi_E$, $\phi_L^+ \rightarrow -\phi_L^+$ or $\phi_L^- \rightarrow -\phi_L^-$. In other words, the kickmap does not depend on the sign of ϕ_E, ϕ_L^+ or ϕ_L^- when only one of them is non-zero.

If we have $\phi_E = 0$ and $-\lambda_p/2 \leq \phi_L^+ \leq \lambda_p/2$ and we transform $\phi_L^+ \rightarrow \phi_L^-$ we have $\Delta x'(x,z) \rightarrow \Delta x'(x,-z)$ and we can use equation 6.16 to show that $\Delta z'(x,z) \rightarrow \Delta z'(-x,z)$. In other words, the coupling terms are reflected but the normal terms are not.

Our study of the kickmap symmetries for an EPU give us greater insight into the effect of the EPU on the electron beam. These symmetries could also be used to speed up some kickmap calculations. We found symmetries of the magnetic field that constrain the kickmaps in the elliptical and linear incline phases. We found transformations of the magnetic field under sign changes in the phases, which relate kickmaps of EPU configurations under sign changes.

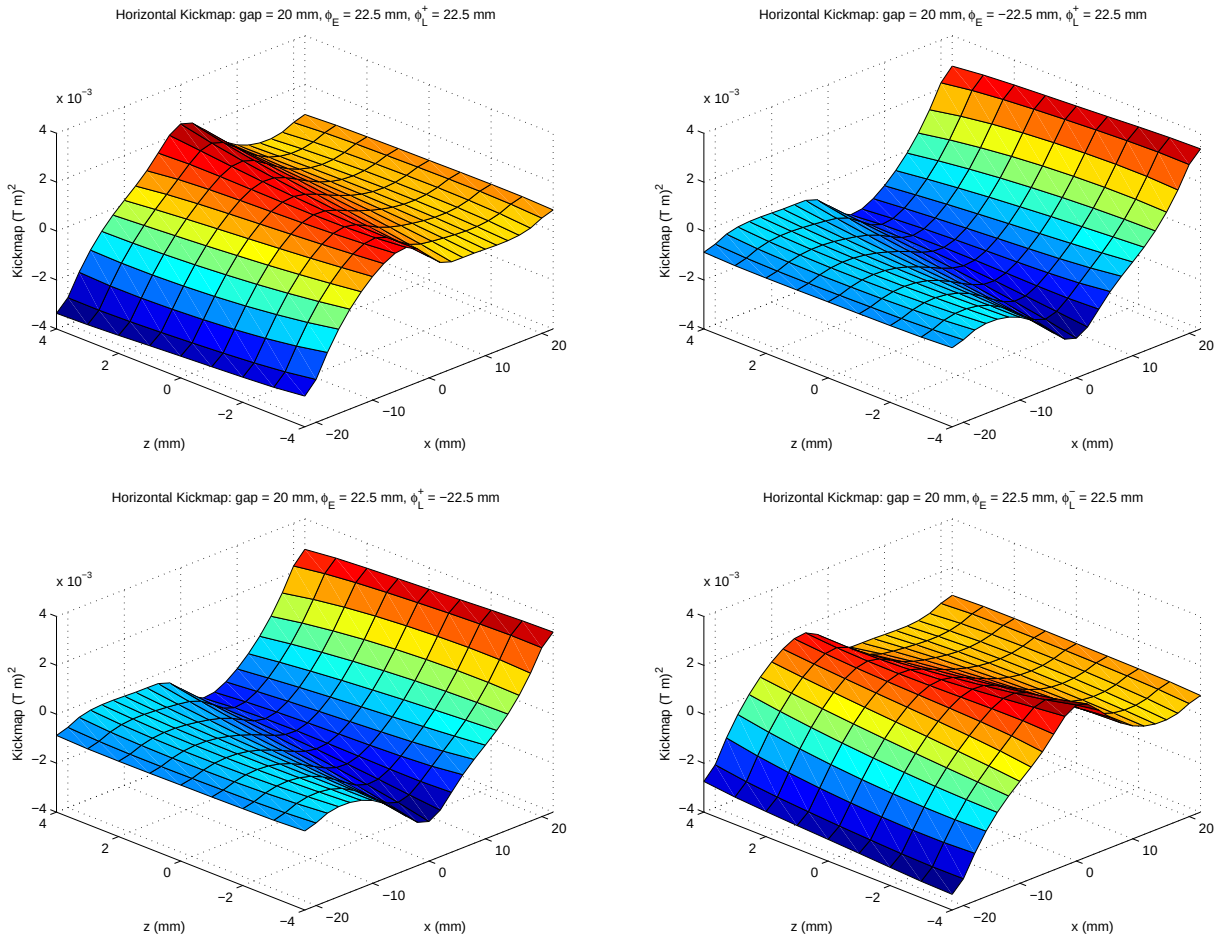

Figure 6.11: Horizontal kickmap $\Delta x'/\alpha^2$ for the EPU of period length $\lambda_p = 180$ mm of Figure 6.2 with phase $\phi_E = \lambda_p/8$ and $\phi_L^+ = \lambda_p/8$ (top left). The transformation $\phi_E \to -\phi_E$ has been applied to the top right figure, while the transformation $\phi_L^+ \to -\phi_L^+$ has been applied to the bottom left figure and the transformation $\phi_L^+ \to \phi_L^-$ has been applied to the bottom right figure.

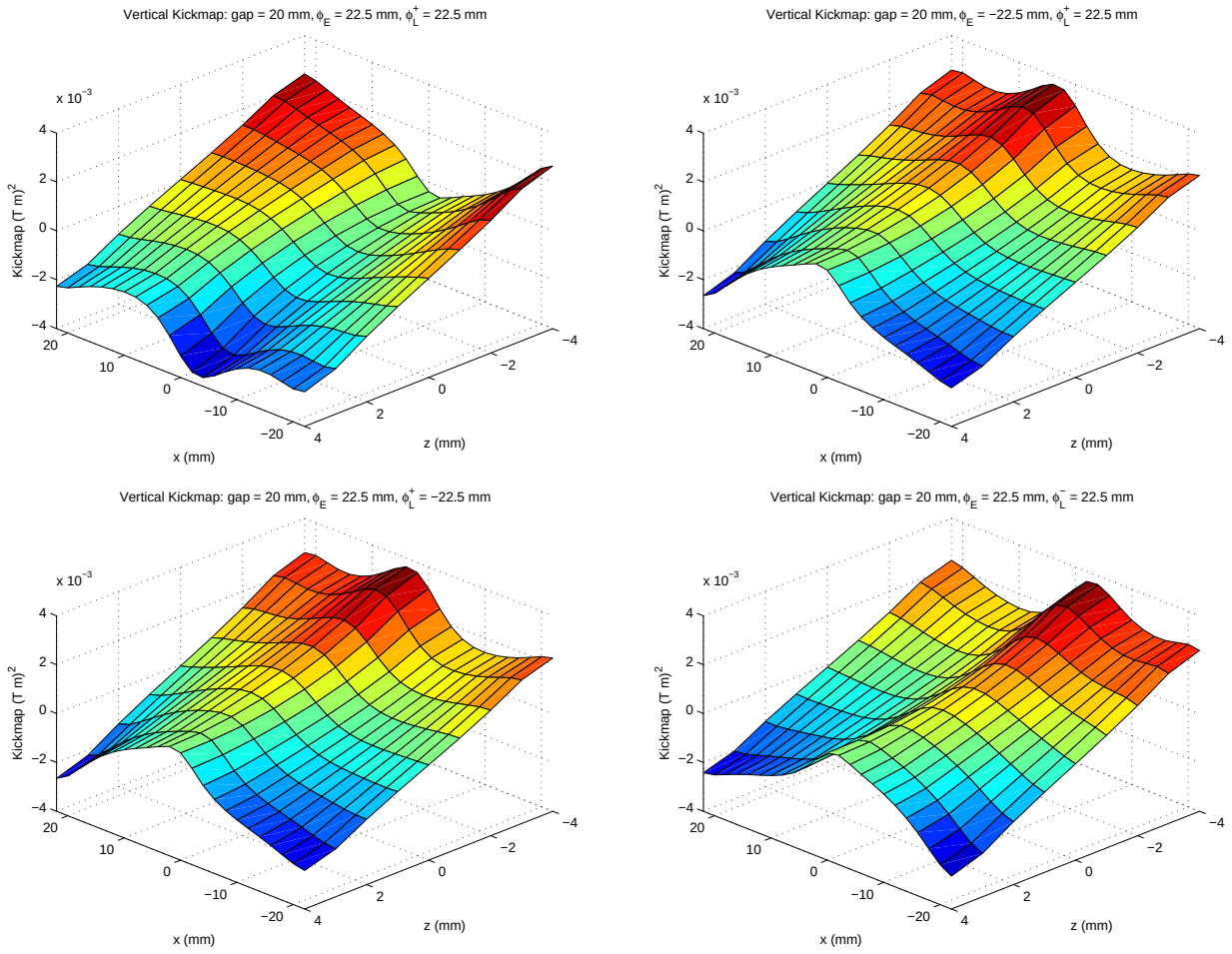

Figure 6.12: Vertical kickmap $\Delta x'/\alpha^2$ for the EPU of period length $\lambda_p = 180$ mm of Figure 6.2 with phase $\phi_E = \lambda_p/8$ and $\phi_L^+ = \lambda_p/8$ (top left). The transformation $\phi_E \to -\phi_E$ has been applied to the top right figure, while the transformation $\phi_L^+ \to -\phi_L^+$ has been applied to the bottom left figure and the transformation $\phi_L^+ \to \phi_L^-$ has been applied to the bottom right figure.

References

[1] P. Elleaume, “A new approach to the electron beam dynamics in undulators and wigglers,” in *Proceedings of EPAC 92*, p. 661, 1992.

[2] P. Elleaume, “Beam displacement and focusing induced by arbitrary field insertion devices,” ESRF Report ESRF-SR/ID-89-33, European Synchrotron Radiation Facility, Dec 1989.

[3] P. Elleaume, O. Chubar, and J. Chavanne, “Computing 3D magnetic fields from insertion devices,” in *Proceedings of PAC 97*, p. 3509, 1997.

[4] M. Borland, “elegant: A flexible SDDS-compliant code for accelerator simulations,” Light Source Note LS-287, Advanced Photon Source, Sept 2000.

[5] H. Wiedemann, *Particle Accelerator Physics II: Nonlinear and Higher-Order Beam Dynamics*. Berlin: Springer, 1995.

[6] J. Safranek, C. Limborg, A. Terebilo, K. I. Blomqvist, P. Elleaume, and Y. Nosochkov, “Nonlinear dynamics in a SPEAR wiggler,” *Phys. Rev. ST Accel. Beams*, vol. 5, p. 010701, Jan 2002.

[7] S. Sasaki, “Analyses for a planar variably-polarizing undulator,” *Nucl. Instr. and Meth. A*, vol. 347, no. 1–3, pp. 83 – 86, 1994.

[8] J. Bahrdt and G. Wüstefeld, “Symplectic tracking and compensation of dynamic field integrals in complex undulator structures,” *Phys. Rev. ST Accel. Beams*, vol. 14, p. 040703, Apr 2011.

[9] T. Schmidt, A. Imhof, G. Ingold, B. Jakob, and C. Vollenweider, “A fixed gap APPLE II undulator for SLS,” in *Ninth Inernational Conference on Synchrotron Radiation Instrumentation*, p. 400, 2006.